bioRxiv preprint doi: https://doi.org/10.1101/168807; this version posted July 26, 2017. The copyright holder for this preprint (which was not certified by peer review) is the author/funder. All rights reserved. No reuse allowed without permission.

PFKFB4 control of Akt signaling is essential for premigratory and migratory neural crest formation.

Ana Leonor Figueiredo[1,2], Frédérique Maczkowiak[1,2], Caroline Borday[1,2],Patrick Pla[1,2], Meghane Sittewelle[1,2], Caterina Pegoraro[1,2], and Anne H. Monsoro-Burq[1,2]*.

[1,] Univ. Paris Sud, Université Paris Saclay, CNRS UMR 3347, INSERM U1021, Centre Universitaire, 15, rue Georges Clémenceau, F-91405, Orsay, France.

[2,] Institut Curie Research Division, PSL Research University, CNRS UMR 3347, INSERM U1021.

* author for correspondence

e-mail: anne-helene.monsoro-burq@curie.fr

Key words.

Neural crest, *Xenopus laevis* embryo, PFKFB, 6-phosphofructo-2-kinase/fructose-2,6-bisphosphatase, AKT, migration, glycolysis, neural plate border.

bioRxiv preprint doi: https://doi.org/10.1101/168807; this version posted July 26, 2017. The copyright holder for this preprint (which was not certified by peer review) is the author/funder. All rights reserved. No reuse allowed without permission.

Summary statement.

PFKFB4 controls neural crest final specification and migration by regulation of AKT signaling or glycolysis.

Abstract.

Neural crest (NC) specification comprises an early phase, initiating immature NC progenitors formation at neural plate stage, and a later phase at neural fold stage, resulting into functional premigratory NC, able to delaminate and migrate. We found that the NC-GRN triggers up-regulation of *pfkfb4* (6-phosphofructo-2-kinase/fructose-2,6-bisphosphatase 4) during this late specification phase. As shown in previous studies, PFKFB4 controls AKT signaling in gastrulas and glycolysis rate in adult cells. Here, we focus on PFKFB4 function in NC during and after neurulation, using time-controlled or hypomorph depletions *in vivo*. We find that PFKFB4 is essential both for specification of functional premigratory NC and for its migration. PFKFB4-depleted embryos fail activating *n-cadherin* and late NC specifiers, exhibit severe migration defects, resulting in craniofacial defects. AKT signaling mediates PFKFB4 function in NC late specification, while both AKT signaling and glycolysis regulate migration. These findings highlight novel and critical roles of PFKFB4 activity in later stages of NC development, wired into the NC-GRN.

bioRxiv preprint doi: https://doi.org/10.1101/168807; this version posted July 26, 2017. The copyright holder for this preprint (which was not certified by peer review) is the author/funder. All rights reserved. No reuse allowed without permission.

INTRODUCTION

The neural crest (NC) is a highly migratory and multipotent cell population of vertebrate embryos, forming an array of differentiated cells: peripheral neurons and glia, pigment cells, craniofacial skeleton, cardiac structures, and endocrine cells (Bronner and LeDouarin, 2012). NC development initiates during gastrulation, at the edges of the neural plate, and continues until late organogenesis. In early gastrulas, NC development is triggered by signals from the adjacent neural plate, non-neural ectoderm, and underlying mesoderm (Saint-Jeannet et al., 1997; Wilson et al., 1997; Neave et al., 1997, Chang and Hemmati-Brivanlou 1998; LaBonne and Bronner-Fraser 1998; Villanueva et al., 2002; Monsoro-Burq et al., 2003; Milet and Monsoro-Burq 2012). These signals specify the neural border (NB), a transition area located across the neural plate and the non-neural ectoderm (Meulemans & Bronner-Fraser 2004; Monsoro-Burq et al. 2005; Basch et al. 2006). In gastrulas, the NB is a mixed territory comprising prospective dorsal neural tube cells, NC and cranial placode progenitors (Steventon et al. 2009, Pegoraro & Monsoro-Burq 2012).

In late gastrulas and early neurulas (i.e. neural plate stage), NC specification is initiated within the NB, upon the coordinated action of WNT signaling and several transcription factors (NB specifiers) broadly activated in this region (PAX3/7, ZIC1/2, MSX1/2, TFAP2A, GBX2, HES4, AXUD, cMYB; Luo et al. 2003; Brewer et al. 2004; Monsoro-Burq et al. 2005; Sato et al. 2005; Khadka et al. 2006; Basch et al. 2006; Nichane et al. 2008; Li et al. 2009; Maczkowiak et al. 2010; de Crozé et al. 2011; Simoes-Costa et al. 2015). This initial phase of NC specification is marked by locally enhanced expression of *tfap2a* and *hes4/hairy2,* and low-level *snail2* and *foxd3,* two transcription factors marking the early NC progenitors, i.e. lineage-restricted cells being still functionally immature (Saint-Jeannet et al. 1989; Essex et al. 1993; Nieto et al. 1994; Mayor et al. 1995; Mancilla and Mayor, 1998; Nichane et al., 2008; de Crozé et al., 2010). During the second half of neurulation, as neural folds elevate, the immature NC is further specified into functional premigratory NC, ready to undergo epithelium-to-mesenchyme transition (EMT) and migration. The fully specified NC (mature) is characterized by late markers *sox10*, *twist* and *tfap2e,* and enhanced *ets1* and *cmyc* (Bellmeyer et al. 2003; Théveneau et al. 2007). In late neurulas, after EMT, NC cells migrate as groups or as individual cells along defined embryonic routes, still expressing *sox10* and *twist* (Theveneau & Mayor 2012). Importantly, TWIST is essential for the coordinated action of EMT regulators SNAIL1/2 (Lander et al. 2013) while enhanced survival properties favors the NC extensive migration (Vega et al., 2004). Finally, the cranial NC populating the craniofacial buds differentiates into mesenchyme, cartilage and bone (Douarin & Kalcheim 1999).

bioRxiv preprint doi: https://doi.org/10.1101/168807; this version posted July 26, 2017. The copyright holder for this preprint (which was not certified by peer review) is the author/funder. All rights reserved. No reuse allowed without permission.

We found that *pfkfb4 (6-phosphofructo-2-kinase/fructose-2,6-bisphosphatase)* expression was upregulated during late NC specification/maturation phase (neural fold stage). In adult cells, PFKFB1-4 control the levels of fructose-2,6-bisphosphate, the strongest allosteric activator of phosphofructokinase1, which regulates the rate-limiting reaction of glycolysis (Okar et al. 2001; Pilkis et al. 1995, Fig.S1). Higher PFKFB4 levels stimulate glycolysis rate. Moreover, in embryos, we have previously shown that PFKFB4 is essential for global ectoderm regionalization. In this context, PFKFB4 acts independently of glycolysis by controlling AKT signaling (Pegoraro et al. 2015). Here, we found that the NC-GRN controls elevated *pfkfb4* expression in the late premigratory NC. Using either constitutive or time-controlled PFKFB4 depletions, and time-controlled pharmacological inhibition of PI3K-AKT signaling *in vivo*, we show that PFKFB4 and AKT signaling regulate a timely switch between lineage-restricted but immature NC and functional premigratory NC. Furthermore, after EMT, PFKFB4, through PI3K-AKT signaling and glycolysis, controls NC migration. These results suggest that NC developmental progression relies upon continuous PFKFB4 function, as a novel NC-GRN actor, whose activity is relayed by AKT signaling.

bioRxiv preprint doi: https://doi.org/10.1101/168807; this version posted July 26, 2017. The copyright holder for this preprint (which was not certified by peer review) is the author/funder. All rights reserved. No reuse allowed without permission.

RESULTS

Pfkfb4 expression labels the neural crest during second half of neurulation.

As in all vertebrate embryos, in *Xenopus laevis,* NB induction starts in early gastrulas (st.10.5 Nieuwkoop-Faber, 1994), as characterized by early expression of *pax3*, *zic1/2*, and *hes4* lateral to the neural plate (Monsoro-Burq et al., 2005; Nichane et al., 2008). NC specification is initiated at the end of gastrulation (st.11.5-12), and is marked by early NC specifiers as *snail2* and *foxd3* at neural plate stage (st.12-14, Fig.1A). NC specification is further established (maturation phase) during neural fold stage (st.14-18), by activation of a later set of NC specifiers and EMT inducers (*sox10, twist)*, and by increased expression of early NC specifiers (Fig.1B). Upon neural tube closure (st.17-19), cranial NC cells undergo EMT and initiate migration to populate the branchial arches and craniofacial areas around tailbud st.24 (Fig.1C).

Among novel genes enriched in premigratory NC, we found *pfkfb4* clustered with *snail2* and *sox10* (Plouhinec et al. 2014). At neural plate stage, *pfkfb4* was expressed at low levels throughout the dorsal ectoderm (Fig.1D). At early neural fold stage (st.14), later than *snail2* initiation, *pfkfb4* was strongly enriched in the NB/NC (Fig.1E,F,L-N). At the end of neurulation (st.18), NC *pfkfb4* mRNA levels, but not *pfkfb1-3* levels, were elevated by 1.5-fold compared to whole embryo expression (Fig.1J, Fig.S2). The premigratory NC expressed 6.4-fold higher *pfkfb4* levels than the adjacent anterior neural fold, which forms forebrain and placodes. Finally, *pfkfb4* was expressed during NC EMT and early migration but decreased as NC cells reached ventral craniofacial areas (Fig.1H-I). This pattern contrasted with blastula and gastrula stages, when low *pfkfb4* levels were detected in the entire dorsal ectoderm, encompassing the neural plate, the NB, and part of the non-neural ectoderm (Pegoraro et al. 2015). Thus, *pfkfb4* was enriched in premigratory NC, during its maturation period, NC EMT and early migration (st14-22).

PFKFB4 activation promotes neural crest formation at the neural border.

Experimental increase of PFKFB4 levels *in vivo* led to a moderate but reproducible increase of the NB and early NC marker expression at the end of neural plate stage (st.14, *pax3, zic1, snail2*, Fig.1O-Q, Table.S2). At the end of neurulation (st.18), the definitive premigratory NC area was also enlarged (Fig.1R,S). In contrast, neural plate specification, anterior-posterior regionalization (*sox2, otx2, hoxb9*) and non-neural ectoderm differentiation (*keratin-K81*) were not affected in late neurulas. We observed a transient and moderate increase of the *sox2*-positive area at mid-neurula stage, which was probably related to the enlarged NB, which transiently expresses *sox2* early on (Fig.1U,W-Y,

bioRxiv preprint doi: https://doi.org/10.1101/168807; this version posted July 26, 2017. The copyright holder for this preprint (which was not certified by peer review) is the author/funder. All rights reserved. No reuse allowed without permission.

Table.S2). Mesoderm formation seemed unaffected (*myod*, Fig.1V). At tailbud stage (st.22-24), migrating NC streams were enlarged with similar ventral migration distance compared to the contralateral control side (Fig.1T,Z). Altogether, *pfkfb4* expression and PFKFB4 gain-of-function phenotype suggested a positive role in NC development. We did not observe ectopic expression of NC markers, in the neural plate or the non-neural ectoderm, suggesting that PFKFB4 was not sufficient to alter specification of adjacent ectoderm cells.

Moderate PFKFB4 depletion affects craniofacial development *in vivo*.

In order to deplete PFKFB4 activity in gastrulas, we previously used a splice-blocking morpholino oligonucleotide (PFKFB4MO, Pegoraro et al. 2015), using 20ng per blastomere in 2-cell-stage embryos. *Pfkfb4* mRNA levels were decreased by 60% (hereafter called severe depletion). Phenotypes were validated using an ATG-targeting and a mismatch morpholino, dose-response, and rescue experiments (Blum et al. 2015). In severe depletion conditions, we observed a developmental blockade before neural fold stage, all dorsal ectoderm cells remaining in an immature progenitor status, while further specification was blocked. Here, in order to analyze later PFKFB4 functions during NC formation, we used two strategies to bypass this early developmental arrest. Firstly, we used low-level PFKFB4 depletion, which no longer blocks ectoderm global developmental progression and allows neurulation to proceed. Secondly, we have used photo-inducible morpholinos, to control PFKFB4 depletion timing *in vivo*, and avoid affecting early development.

Based on *pfkfb4* enhanced NC expression, we hypothesized that NC development required maintenance of high PFKFB4 levels, while other tissues may develop normally under mild PFKFB4 depletion conditions. Using decreasing PFKFB4MO doses, we created mild hypomorph conditions (about 35% decrease in *pfkfb4* mRNA level, Fig.2A), and monitored the craniofacial morphology and pigmentation phenotype of st.45 tadpoles (Fig.2B-E). We found that low-level depletion (injecting 5ng of MO into one dorsal-animal blastomere, at the 4-cell stage or any equivalent combination at other developmental stages), resulted in a morphologically normal gastrulation and neurulation but caused a significant reduction of head structures on the injected side, compared to the uninjected side (Fig.2B). Pigment cells were present on both sides of the tadpoles and appeared unperturbed. Lower morpholino doses (2.5ng or 1ng in one of four blastomeres) did not significantly alter embryo morphology. Higher doses caused early death of the injected cells (this apoptosis was rescued by adding *pfkfb4* mRNA as described in Pegoraro et al., 2015). With the low-level PFKFB4 depletion, we checked that injected cells were not subjected to increased cell death compared to control cells in the vast majority of the embryos (Fig.S3). Moreover, neither ventral injections of PFKFB4MO nor dorsal

bioRxiv preprint doi: https://doi.org/10.1101/168807; this version posted July 26, 2017. The copyright holder for this preprint (which was not certified by peer review) is the author/funder. All rights reserved. No reuse allowed without permission.

injections of a non-related MO (even at high doses) caused cell death, excluding non-specific effects of morpholino injection (Fig.S3). These observations confirmed the hypothesis that NC development was specifically affected by low-level depletion of PFKFB4. Therefore, using these hypomorph PFKFB4 conditions, we could explore the roles of PFKFB4 in NC derivatives formation *in vivo*. All further experiments, except for photo-morpholinos, were thus conducted using this low MO concentration.

The NC generates most craniofacial structures including craniofacial skeleton, mesenchyme and soft tissues around the eyes. Following moderate PFKFB4 depletion, dorsal and ventral craniofacial structures were globally smaller. On the morphant side, branchial cartilages were strongly reduced while Meckel's and ceratohyal cartilages were moderately diminished (Fig.2C-E). Eyes were also affected, with grossly normal shape but reduced size. Since *pfkfb4* is present at low levels in the neural plate early on (Fig.1), this could be due to a cell autonomous defect in the optic vesicles forming from the neural plate. Alternatively, CNCC defects could influence the developing eye (Bailey et al. 2006; Lwigale 2015). Hence, the NC-derived craniofacial structures were severely affected when PFKFB4 levels were downregulated moderately while most other structures were normal.

PFKFB4 depletion affects premigratory neural crest specification and NCC migration.

We then investigated which steps of NC formation were affected by PFKFB4 low-level depletion. At early neural fold stage, *snail2* expression was very low to absent on the injected side (Fig.3A,L-first bar, Table.S2). This defect was a delay, since, by the end of neurulation, most embryos expressed *snail2* normally (Fig.3B,L). In theory, delayed *snail2* activation could be followed by either the later onset of the entire NC specification cascade or by globally defective NC development. To assess definitive NC specification at the end of neural fold stage, we analyzed expression of late NC specification markers, *sox10* and *twist*. While *sox10* was normally activated (Fig.3C), *twist* expression was severely defective (Fig.3D) and *hes4*, marking immature premigratory NC was increased (Fig.3E, Table.S2). In contrast, neural ectoderm, non-neural ectoderm and paraxial mesoderm specification were unaffected (*sox2, ep.ker.*, *myod*, Fig.3I-L, Table.S2). Neurulation and neural tube closure were slightly delayed on the injected side, but neural tube eventually closed (Fig.3.G,I). Importantly, while some neural border markers were expressed normally at the time of neural tube closure (e.g. *msx1,* Fig3.H), others were moderately (*zic1)* to strongly increased (*pax3)* suggesting that the NC cells had partially retained an immature NB-like character, at a developmental stage when they should have been specified into functional premigratory NC (Fig.3H,I).

bioRxiv preprint doi: https://doi.org/10.1101/168807; this version posted July 26, 2017. The copyright holder for this preprint (which was not certified by peer review) is the author/funder. All rights reserved. No reuse allowed without permission.

After neural tube closure and NC delamination, low-level PFKFB4 depletion resulted in severely defective NC migration, both with diminished expression of migrating NC markers *(twist, sox10)*, and decreased migration distance towards the facial areas of the cells expressing these markers (Fig.3M-S). Although the percent of embryos with abnormal *twist* expression was slightly lower than at the end of neurulation (Fig.3S-st.24, Fig.3L-st.18), these results indicated that defects and delay in premigratory NC specification were not compensated at the subsequent stage of NC migration. At this stage, the central nervous system and the optic vesicle were grossly normal (*sox2,* Fig.3R). When PFKFB4 morphant phenotype specificity was assessed, by co-injecting PFKFB4MO with *pfkfb4* mRNA, the morphant phenotype was rescued during NC specification and migration (Fig.3S, Fig.S4, and not shown).

Altogether, these results indicated that a moderate loss of PFKFB4 activity resulted in a strong impediment of NC development. The NC territory was established, identified by *sox10* expression and outlined by *msx1* expression (Fig.3C,H). However, its specification was delayed at neural plate stage (*snail2)*, which was incompletely compensated at late neural fold stage (defective *twist,* increased *hes4*), accompanied by the retention of NB-like character (increased *pax3*) in premigratory NC. This was followed by defective migration of *sox10/twist*-expressing NCC in tailbud stage embryos. As a result, fewer *twist*- or *sox10*-positive cells populated the craniofacial buds. These alterations were sufficient to explain the morphological craniofacial defects observed at st. 45 (Fig.2). However, using the constitutively active PFKFB4MO, we could not distinguish between an early need for PFKFB4 during NC specification, causing defective NC migration, and a continuous need for PFKFB4 activity during NC specification and migration.

Inducible PFKFB4 depletion affects neural crest specification and its migration *in vivo*.

To understand PFKFB4 function at each step of NC formation, we set up an inducible knockdown strategy, using a UV-cleavable sense morpholino (PFKFB4-PhMO) that blocked *pfkfb4* antisense MO until UV exposure. Although more fragile, we injected albino embryos for UV penetration. The uninjected side controlled for non-specific UV effects. As control, severe PFKFB4MO constitutive depletion led to abolished or severely decreased *twist* expression (in 80% and 17% of embryos, Fig.4A-C,H). PFKFB4-PhMO/MO co-injections efficiently blocked the severe morphant phenotype (uninduced embryos, u.i.): *twist* was normally expressed in 60% of st.18 embryos. Despite minimal ambient light throughout experiments, we observed some leakage in the PhMO/MO u.i. condition, leading to 22.5% of embryos with severe decrease in *twist* expression and 17.5% with mild defects. However, after UV exposure upon injection (a.i., illumination at the 4-cell stage), *twist*

bioRxiv preprint doi: https://doi.org/10.1101/168807; this version posted July 26, 2017. The copyright holder for this preprint (which was not certified by peer review) is the author/funder. All rights reserved. No reuse allowed without permission.

expression decreased significantly on injected side in 73% of embryos (Fig.4H). The lower efficiency of the PhMO/MO a.i. condition compared to the constitutive PFKFB4MO phenotype, leading to only 26% of embryos with severe *twist* blockade and 47% with mild defects, could be due to a partial *pfkfb4-PhMO* cleavage, leading to a hypomorph phenotype. Indeed, the embryos exhibited malformations similar to the ones observed at low doses with constitutive depletion (Fig.3).

To study PFKFB4 role during NC specification, embryos were UV-illuminated at the end of gastrulation (st.12.5), and analyzed at late neural fold stage (st.18). Before induction, development appeared normal (*sox2, ep.ker.* expression, not shown). PFKFB4 knockdown from st.12.5 resulted in a significant *twist* downregulation (Fig.4D-H) compared to injected but uninduced embryos. Therefore, PFKFB4 plays a specific role during NC specification, distinct from its early function on ectoderm patterning during gastrulation. Moreover, this effect mirrors the hypomorph phenotype observed with the mild PFKFB4 depletion (Fig.3).

PFKFB4 knockdown was then induced at late neural fold stage, as NC cells have completed specification, maturation and initiated EMT (st.18). Before illumination, development was mainly normal, despite slightly decreased *twist* expression (u.i., Fig.4H). In st.24 tadpoles, we analyzed *twist* expression, NC streams shape and migration distance from the dorsal midline. *Twist* was normal in embryos injected with *lacZ* or PhMO/MO uninduced, while the injected cells were lacking (eliminated after cell death) in PFKFB4MO-injected embryos (Fig.4I-N,U). After st.18 photo-induction, *twist* was significantly altered in 69% of embryos (Fig.4O-U). For the milder phenotype ("migration", 21%), tadpoles presented a modestly reduced migration distance (13% reduction), with a robust *twist* expression but smaller NC streams (17% area reduction). This limited effect was reproducible and statistically significant, compared to variations observed in *lacz*-injected embryos or the injected embryos classified as normal (Fig.4O,P,V,W). The second phenotype ("migration and staining", 28.5%) presented similarly reduced migration distance (14% reduction) but more intense decrease in NC streams area (34% smaller) and lower *twist* staining intensity (Fig.4Q,R,V,W). Finally, 19% of the embryos exhibited strongly reduced *twist* expression ("severe staining defect"), with 36% reduced area, the low staining preventing measure of migration distance (Fig.4S,T,V,W). Hence, depleting PFKFB4 after NC specification, at the time of EMT, affected *twist* expression, the size of NC streams, and NC migration distance.

Together, these results demonstrated a requirement for PFKFB4 function at two successive and distinct steps of NC development: patterning of mature NC during neurulation and NC migration

bioRxiv preprint doi: https://doi.org/10.1101/168807; this version posted July 26, 2017. The copyright holder for this preprint (which was not certified by peer review) is the author/funder. All rights reserved. No reuse allowed without permission.

at tailbud stage. Moreover, these effects closely mimicked those observed after low-level PFKFB4 depletion.

PFKFB4 controls AKT signaling in premigratory NC.

PFKFB4 regulation of glycolysis, as seen in adult cells, was not involved in neural crest late specification, since glycolysis blockade during neural fold stage did not alter *twist* expression (Fig.S5, other markers not shown). In order to understand how PFKFB4 may affect NC late specification, we assessed cell signaling parameters and cell proliferation in premigratory NC. In gastrulas, PFKFB4 levels impact PI3K-AKT signaling. Here, to address precisely the level of AKT signaling in developing neural crest progenitors, we dissected out either the neural border territory at the end of neural plate stage, or the premigratory cranial neural crest at the end of neural fold stage, and measured phospho-SER473-AKT levels in control and PFKFB4 hypomorph conditions. AKT signaling was specifically decreased in morphant NC progenitors compared to controls (Fig.5A)

AKT signaling regulates many aspects of cell homeostasis, including cell proliferation. We next wondered if the rate of cell proliferation was affected in morphant NC, and if the pool of *cmyc*-positive NC stem cells was normal (Bellmeyer et al. 2003). After EdU incorporation, we observed normal cell proliferation on the morphant side (Fig.5B). *Cmyc* expression was normal on the morphant side, when *twist* was defective in sibling embryos (Fig.5C,D). Together, these results suggested that the morphant territory generates a rather normal pool of NC stem cells, suggesting that the phenotype relies on genuine patterning defects within a partially specified NC domain.

To assess if diminished AKT signaling was sufficient to affect NC specification and maturation, and to phenocopy the morphant phenotype, we treated embryos with PI3K-AKT inhibitor (LY294002, 40-80μM). As a comparison, we used a MAPK/ERK inhibitor (UO126, 40-80μM) since both AKT and MAPK signaling pathways are often activated downstream of tyrosine kinase receptor signaling. Each treatment was checked for inhibition of p-ERK and p-AKT (on whole embryo lysates, not shown). Embryos were treated exclusively during neural fold stage (from st.14 to st.18). Inhibiting PI3K-AKT signals blocked *twist* but not *cmyc* induction. In contrast ERK inhibitor had no effect on either gene expression (Fig.5E-H). This result showed that AKT signaling was specifically needed during the last phase of premigratory NC maturation. When AKT function was disrupted, a normal pool of *cmyc*-positive NC stem cells formed but they failed expressing the late NC specifier *twist*.

bioRxiv preprint doi: https://doi.org/10.1101/168807; this version posted July 26, 2017. The copyright holder for this preprint (which was not certified by peer review) is the author/funder. All rights reserved. No reuse allowed without permission.

Finally, when a constitutively active form of AKT was co-injected with PFKFB4MO, *twist* specification defects were rescued, demonstrating that the main cause of PFKFB4 morphant phenotype prior to migration, was due to altered AKT signaling (Fig.5I-J).

PFKFB4 depletion affects neural crest EMT and migration in a cell autonomous manner.

To understand the defects during NC EMT and migration upon PFKFB4 low-level depletion, we reasoned that morphant NC cells, with delayed or incomplete specification (Fig.3), might require longer time than wild-type NC to mature and undergo migration. Additionally, interactions between the NC and its *in vivo* environment are essential for migration. Using the more robust pigmented frog embryos, we challenged the ability of morphant NCC to migrate in a wild-type host environment (Fig.6). We implanted GFP-labeled premigratory morphant NC into a stage-matched wild-type host and followed cell migration *in vivo*. In contrast to the control wild-type grafts which healed within 20 minutes after transplantation, the morphant tissue healed with difficulty: most of the donor tissue failed to adhere to the host tissues, even as long as two hours post grafting (not shown). Moreover, after healing, the vast majority of the grafted morphant cells failed to migrate although occasional cells could be traced in the mandibular arch area (Fig.6C-D, compare to wild-type cells in A,B). This phenotype was qualitatively similar to the defects observed in the morphant embryos (Fig.4), either with constitutive or inducible morpholinos. In this transplantation assay, however, the lack of migration was observed in a higher number of cases, possibly because of the additional healing defect revealed by the assay. This challenge revealed that PFKFB4 morphant cells displayed altered healing and survival ability upon EMT and migration stage.

We further analyzed the fate of the morphant cells *in vivo* with another strategy. In order to avoid interference with altered healing properties, we traced the injected cells with *gfp* mRNA co-injected with PFKFB4MO, by targeting dorsal-animal blastomere D1.2 at stage 8 to 16 cells, which mostly forms dorsal neural tube and NC progenitors (Moody et al., 1987). We followed the fate of NC progenitors, by selecting embryos with GFP-positive premigratory NC at the end of neurulation (st.18, Fig.6F-H). In these conditions, without further experimental manipulation of the injected cells, we find that the control cells undergo EMT, migrate and populate efficiently craniofacial areas as expected, while morphant cells fail to do so in a dose dependent manner. In contrast, the morphant cells contribute to brain and eye as efficiently as control cells (Fig.6G,I,J). We concluded that the defective NC specification and maturation, observed at st.18, was not compensated later on, even when morphant cells face a wild-type environment, and that a lower PFKFB4 activity resulted in a cell-autonomous alteration of NC ability to undergo EMT and migration *in vivo*.

bioRxiv preprint doi: https://doi.org/10.1101/168807; this version posted July 26, 2017. The copyright holder for this preprint (which was not certified by peer review) is the author/funder. All rights reserved. No reuse allowed without permission.

To understand the cellular and molecular basis of morphant NC phenotype, we tested adherence, EMT and migration on fibronectin *in vitro* (Fig.6K-R). This assay was done using earlier tissue than in previous publications, i.e using neural border at st. 14 instead of premigratory NC st.17-18, which has already started EMT. Doing so, this assay allows visualizing separately adherence a few minutes after plating, then EMT about 2 hours after plating, and finally cell migration on the fibronectin substrate starting 3,5-4hours after plating (Fig.6K-N). Morphant neural folds were thus dissected out at the end of neural plate stage (st.14). They failed to adhere efficiently on fibronectin, did not undergo EMT (O-P) and poorly migrated (Q-R), while wild-type neural folds adhered, underwent a very clear EMT (K-L), dispersed and actively migrated (Fig.6M-N)). A key parameter for NC EMT is the up-regulation of *n-cadherin* expression prior to EMT (Theveneau & Mayor 2012). We found that *n-cadherin* expression levels were significantly lower in morphant NB (st.14) and NC (st.18) compared to stage-matched controls (Fig.6E).

We concluded that lower PFKFB4 activity resulted in premigratory NC with defective *n-cadherin* levels. These cells were unable to undergo EMT on a fibronectin substratum *in vitro*, exhibited poor ability to adhere, heal, or migrate upon grafting in wild-type host environment *in vivo.* The morphant cells remained integrated into adjacent tissues such as central nervous system or eye. These altered capacities were sufficient to explain the late phenotype in tadpoles, with underdeveloped craniofacial structures.

At tailbud stage, PFKFB4 depletion alters both glycolysis and AKT signaling, which together impact NC migration.

PFKFB4 depletion decreased glycolysis in embryos (Fig.S5). To understand PFKFB4 depletion phenotype during NC migration, we blocked either glycolysis or AKT signaling from EMT stage (st.18) to migration into branchial buds (st.24) (Fig.7, S6). Glycolysis was blocked using 2-deoxyglucose (2DG), a non-hydrolysable glucose. The PI3K inhibitor LY294002 was used at various doses to block PI3K-AKT signaling. Efficiency of each treatment was monitored (Fig.S5). We found that both glycolysis and AKT phosphorylation blockade from st.18 to st.24, resulted into severe disruption of NCC migration, (*twist, sox9, sox10,* Fig.7, Fig.S6). The effects of LY294002 were dose-dependent (not shown). While glycolysis blockade seemed to mainly affect NC streams morphology, AKT inhibition also affected general embryo development (not shown). In order to test for delayed NCC migration and for general treatment toxicity, embryos were transferred in drug-free medium from tailbud st.24 until late tadpole st.45. In these conditions, potential delays would be compensated, while general toxicity would lead to embryo death. Here, embryo survival was normal. St.45

bioRxiv preprint doi: https://doi.org/10.1101/168807; this version posted July 26, 2017. The copyright holder for this preprint (which was not certified by peer review) is the author/funder. All rights reserved. No reuse allowed without permission.

craniofacial morphology was analyzed. Relative to body size, heads were smaller and visceral cartilage elements were severely underdeveloped as observed upon PFKFB4 depletion, especially after AKT signaling blockade. Interestingly, combining both glycolysis and AKT blockade led to stronger craniofacial phenotype, suggesting cooperation of the two processes (Fig.S6). We concluded that blocking AKT signaling or, with less efficiency, blocking glycolysis, phenocopied PFKFB4 morphant phenotype during NC migration. Both AKT signaling and glycolysis were thus needed for a large number of NCC to populate the branchial arches and head structures.

Since AKT blockade seemed most effective in mimicking PFKFB4 depletion, we attempted to rescue the craniofacial phenotype by co-injecting *caAkt* mRNA with PFKFB4MO. By st.45-46, we observed that constitutive activation of AKT signaling alone did not affect craniofacial development (Fig.7N,P). While morphant injected sides were severely reduced (Fig.7M,P), most tadpoles co-injected with PFKFB4MO and *caAkt* were symmetrical (Fig.7O,P). This experiment demonstrated that defects of NC craniofacial derivatives observed upon PFKFB4 depletion were largely due to loss of AKT phosphorylation and were efficiently compensated by restoring active AKT signaling.

The NC-GRN regulators control *pfkfb4* activation at the neural-non-neural border.

Finally, we analyzed *pfkfb4* upregulation at the edges of the neural plate. We asked if the NC-GRN actors actively controlled *pfkfb4* expression, as they do for *snail2,* either during early *pfkfb4* activation in the end of neural plate stage, or in premigratory NC. We used MO-mediated depletions with well-established morpholinos, dominant-negative constructs (Fig.8) or gain-of-function experiments (Fig.S7). First, the secreted NC inducers, including WNT and FGF8 signals as well as modulating BMP signaling, affected similarly *snail2* and *pfkfb4* (Fig.8A-L, Fig.S7). Secondly, we found that the key transcription factors acting at the NB to specify NC, PAX3 and TFAP2a, were also essential to establish *snail2* and *pfkfb4* (Fig.8M-T, Fig.S7). In addition, the NC specifier SOX9 was needed for expression of both genes at the NB and in premigratory NC (Fig.8U-X). All these results indicated that increased *pfkfb4* expression in the NC progenitors is actively promoted by the NC-GRN regulators, as for more classical partners of the network (e.g. *snail2)*. Thus, our results show that PFKFB4 key function, which mainly relies on ensuring proper AKT signaling in NC progenitors, is encoded within the NC-GRN. PFKFB4 could be a major intermediate actor in NC control by WNT-FGF-BMP signals.

DISCUSSION

bioRxiv preprint doi: https://doi.org/10.1101/168807; this version posted July 26, 2017. The copyright holder for this preprint (which was not certified by peer review) is the author/funder. All rights reserved. No reuse allowed without permission.

In this study, we have evidenced that PFKFB4 activity is required continuously during several key steps of NC formation: during premigratory NC maturation at neural fold stage, and during NC migration towards the craniofacial buds at tailbud stage. This activity is critical as PFKFB4 depletion led to hypomorphic craniofacial structures. We showed that the major transcription factors and signaling pathways that control the NC-GRN, control *pfkfb4* activation in NC progenitors during neural fold stage, i.e. during the phase of NC maturation. In turn, PFKFB4 controls AKT signaling activity in NC, which is essential for NC maturation and migration. PFKFB4 is a known glycolysis regulator, and its depletion in neurulas affected glycolysis. However, at neural fold stage, glycolysis is not required for NC patterning. In contrast, at tailbud stage, both AKT signaling and glycolysis are important parameters to ensure NC migration. Finally, restoring AKT signaling compensates PFKFB4 depletion and results in normal craniofacial development. This indicates that PFKFB4 critical action on NC development is mainly mediated by its action on AKT signaling (Fig.9).

The enzyme PFKFB4 is an integral partner of the NC-GRN. While it is ubiquitously expressed in the dorsal ectoderm at gastrulation stage (Pegoraro et al., 2015), we found that, during neurulation, *pfkfb4* expression is upregulated in immature NC progenitors, starting at neural fold stage. *Pfkfb4* is further expressed in the NC initiating their migration (Fig.1. We have shown that the major NC-GRN regulators, including secreted inducers, NB specifiers, and NC specifiers, control *pfkfb4* expression in the neural folds (Fig.8). Moreover, depletion of PFKFB4 did not prevent NB specifiers expression but led to delayed or decreased expression of early (*snail2)* and late *(twist)* NC specifiers (Fig.3). According to the hierarchical model of the NC-GRN, this indicated that PFKFB4, while not a transcription factor, acts as a NC specifier (Betancur et al. 2010; Milet & Monsoro-Burq 2012). The maintenance of *pfkfb4* expression in NC could further involve NC-GRN actors. We have evidenced that PFKFB4 was needed reiteratively during NC specification and migration (Figs.4,6). Likewise, WNT and TFAP2a function are also needed at successive steps of NC formation (LaBonne & Bronner-Fraser 1998; Monsoro-Burq et al. 2005; Simões-Costa et al. 2015; Luo et al. 2003; de Crozé et al. 2011). Both WNT signals and TFAP2a activate *pfkfb4* expression during NC specification, suggesting that they could potentially sustain its expression also during later NC development.

Our data suggest that the main function of PFKFB4 upregulation in premigratory and migratory NC is to ensure optimal AKT signaling levels in these cells (Fig.5, 7). We also show that blocking AKT signaling in temporally controlled conditions, affects NC specification and migration independently (Fig.5, 7). In mouse embryos, a recent study also demonstrated importance of AKT signaling for NC migration: *Specc1l* mutants or knockdowns exhibit defective neural tube closure and cranial NC

bioRxiv preprint doi: https://doi.org/10.1101/168807; this version posted July 26, 2017. The copyright holder for this preprint (which was not certified by peer review) is the author/funder. All rights reserved. No reuse allowed without permission.

409 migration, with decreased phospho-AKT levels. In this context also, activating PI3K-AKT signaling
410 rescued the phenotype (Wilson et al. 2016). Together these data suggest that the acute need for
411 optimal AKT signaling during NC migration might be conserved in amniote and non-amniote
412 vertebrates.
413
414 The regulation of NC early development by PFKFB4 and AKT was essential to shape the
415 embryonic head. We propose that it ensures that numerous NCC populated the branchial arches, and
416 differentiated into cartilage elements with appropriate size rather than impacting the morphogenesis of
417 these elements (Fig.2, 7). When inducible depletion was performed during NC migration only, cells
418 eventually migrated almost down to the target tissues, but in smaller numbers (Fig.4). Neural tube
419 closure and craniofacial defects are an acute societal issue for human health. Hypomorphic
420 craniofacial structures, especially for the jaw, are observed in many human syndromes, and not yet
421 linked to specific mutations (reviewed in Heike et al. 1993). Our study shows that impaired AKT
422 signaling, specifically in the NC progenitors by means of PFKFB4 depletion, creates reduced jaw and
423 branchial arches structures. This could happen because defects arose at time of NC specification, or
424 during its migration. Our results thus show that even modest reduction of PFKFB4 levels, or of AKT
425 signaling, when applied during developmental periods corresponding to critical steps of NC
426 development, results into severe craniofacial defects. This study highlights the importance of a strict
427 temporal schedule during NC developmental cascade. This schedule culminates with the EMT and
428 migration onset of mature NC cells in register with neural tube closure. Optimal AKT signaling,
429 regulated by high PFKFB4 levels, ensures that no delay in this developmental cascade occurs, that
430 immature progenitor (NB-like) characters are not retained, and that the ultimate molecular switches
431 (*twist and n-cadherin* expression) are activated in a timely manner, allowing NC to undergo EMT upon
432 neural tube closure. Later on, PFKFB4 and AKT signaling further optimize the efficiency of NC cell
433 migration towards the branchial arches. Similarly, AKT signalling was recently shown to up-regulate *n-*
434 *cadherin* and control NC migration downstream of PDGF-A/PDGFRa (Bahm et al., 2017). This
435 suggests that various cell inputs use AKT signaling as a hub to control NC formation.
436
437 During NC migration, our results outlined a potential link between PFKFB4, AKT and
438 glycolysis, because AKT activation rescued the global *pfkfb4* morphant phenotype (lower AKT
439 signaling and lower glycolysis rate, Fig.5, 7). We conclude that AKT compensates all aspects of
440 PFKFB4 depletion, directly or indirectly. In adult cancer cells and stem cells, PI3K/AKT signaling
441 regulates glycolysis, which controls tumor cell motility (Han et al. 2013; Ito & Suda 2014; Courtnay et
442 al. 2015). This mechanism could be involved in NC, as forced AKT signaling rescues PFKFB4

bioRxiv preprint doi: https://doi.org/10.1101/168807; this version posted July 26, 2017. The copyright holder for this preprint (which was not certified by peer review) is the author/funder. All rights reserved. No reuse allowed without permission.

phenotype. Comparison with cancer cells further highlight potential common mechanisms. In tumors, glycolysis enzymes are multifunctional regulators, which impact on cell physiology in addition to their role in glycolysis. For example, Alpha-enolase regulates PI3K-AKT signaling and downstream cell EMT regulators such as *snail1* and *n-cadherin* in lung cancer (Fu et al. 2015). PFKFB3 controls PI3K-AKT in human osteoarthritis cartilage, in adipocytes and in cancer cells (Trefely et al. 2015; Qu et al. 2016). It has been proposed recently, that increased aerobic glycolysis in tumor cells (Warburg effect) promotes cell survival and cell cycle by stimulating IGF/AKT signaling, in addition to its role in cellular energy and metabolic intermediate production (Trefely et al. 2015). Our findings highlight a novel embryonic process, essential for NC EMT and migration, which parallels some mechanisms of cancer progression. It was shown that migrating NC cells displayed increased resistance to multiple cell stresses (Vega et al. 2004), ensuring their optimal long distance travel throughout various embryonic environments. Altogether, our findings show how these properties are acquired and sustained, during and after premigratory NC maturation, and how they are encoded in the NC-GRN, using unconventional function of a glycolysis regulator to control AKT signaling.

MATERIALS AND METHODS

All morpholinos, plasmids and reagents are described in Table S1.

Embryos, microinjection, NB culture and NC grafts.

Pigmented and albino *Xenopus laevis* embryos were obtained and staged using standard procedures (Sive et al. 2010) (Nieuwkoop & Faber 1994). European and National Regulation for the Protection of Vertebrate Animals used for Experimental and other Scientific Purposes were strictly applied (licence #C91-471-108, *Direction Départementale de Protection de la Population, Courcouronnes,* France). MOs or mRNAs were co-injected with *NLS-lacZ* mRNA or *histone2B-gfp* mRNA for lineage tracing. Bgalactosidase activity, revealed in red, marked the injected side. Embryos were injected unilaterally for WISH/morphology or on both sides (for western-blot and RTqPCR).NB and NC culture/grafting experiments were described in (Milet & Monsoro-Burq 2014).

Plasmids and morpholinos

mRNAs were obtained *in vitro* (mMessage mMachine SP6 or T7 kits, Ambion). UV-cleavable photomorpholino (PhMO) experiments were performed on albino embryos (molecular ratio of sensePhMO/splice-blockingMO=1.25). PhMO cleavage was induced by 15 min UV exposure using a HBO 103W/S source.

bioRxiv preprint doi: https://doi.org/10.1101/168807; this version posted July 26, 2017. The copyright holder for this preprint (which was not certified by peer review) is the author/funder. All rights reserved. No reuse allowed without permission.

Pharmacological treatments

Glycolysis, MAPK and PI3-Akt signaling were inhibited using 2-deoxyglucose (Sigma), UO126 or LY294002 (Sigma) respectively, on batches of 50 sibling embryos. Lactate concentration was measured on 20-40 embryos (L-Lactate Kit, Abcam).

Cell proliferation and cell death assays

Cell proliferation was assessed based on EdU incorporation for 2 hours (1mM EdU injected ventrally into st. 18 embryos, Molecular Probes). Either *gfp* mRNA alone, or PFKFB4MO and *gfp* mRNA were injected unilaterally. Serial paraffin sections were immunostained. A minimum of 130 cells in the territory corresponding to the neural crest was counted on the GFP-injected side, compared to the contralateral side. Cell death was assessed by activated caspase 3 immunostaining *in toto*.

Cartilage staining

Embryos were stained with 0.05% Alcian blue, destained in ethanol, rehydrated and cleared with 4% KOH then in graded glycerol solutions. Cartilages were manually dissected out.

Whole-mount in situ hybridization (WISH) and sectioning

We used a procedure optimized for NC (Monsoro-Burq 2007). For sectioning, embryos were embedded in gelatin-albumin. 30 μM thick vibratome transverse sections were cut.

Western blotting

Lysates (5-10 whole embryos, 10-15 NBs, NCs or dorsal explants) were prepared using phosphatase (PhosSTOP, Roche) and protease-inhibitors (Sigma) and analysed by standard western blotting.

RT–qPCR

Total RNA was extracted from 3-5 whole embryos or 5 NB, NC or dorsal explants (Sive et al, 2000). RT–qPCR was performed according to standard procedures using MIQE recommendations. Results were normalized against the reference genes *odc* and *ef1a*. Primers used to test PFKFB4MO efficiency span the exon1-exon2 region, i.e. include the exon1-intron1 junction targeted by the morpholino.

Statistical analysis, imaging and image processing.

All experiments were performed at least three times independently (except duplicates for Figs. 5A). The most frequent phenotypes are shown. Graphs indicate the mean percentage of embryos for a

bioRxiv preprint doi: https://doi.org/10.1101/168807; this version posted July 26, 2017. The copyright holder for this preprint (which was not certified by peer review) is the author/funder. All rights reserved. No reuse allowed without permission.

given phenotype. NC stream area and NC distance of migration was measured (Fig. 4, ImageJ software). Error bars = SEM. Student's t-test was used (p-value ≤0.05). Images were processed with standard calibration of RGB levels (Photoshop, Gimp).

ACKNOWLEDGEMENTS

The authors are grateful to all members of the Monsoro-Burq team and to S. Saule for interactive discussions and R. Harland for gift of plasmids. We specially thank C. Milet, A. Valluet and A. Dolly for initiating the Akt analysis, C. Pouponnot and A. Eychène for IP experiment. We thank the PICT-IBiSA imaging facility for technical advice and E. Belloir and C.Alberti for *Xenopus* husbandry.

COMPETING INTERESTS

The authors declare no competing or financial interests.

AUTHOR CONTRIBUTIONS

A.L.F, F.M, C.B, P.P, C.P, M.S. and A.H.M.B designed, conducted and analyzed the experiments. A.L.F, F.M, C.B, P.P, M.S. and A.H.M.B have discussed the results and written the manuscript.

FUNDING

This study was supported by funding from Université Paris Sud, CNRS, Association pour la Recherche contre le Cancer (ARC PJA20131200185), Agence Nationale pour la Recherche (ANR Programmes Blanc CrestNet and CrestNetMetabo), and Fondation pour la Recherche Médicale (FRM, Programme Equipes Labellisées DEQ20150331733, DGE20111123020). A.L. Figueiredo was a PhD fellow of the French Ministry for Research and Education (MENRT) and Fondation pour la Recherche Médicale (FDT20140930900). M.S. was a Ph. D. fellow funded by Fondation pour la Recherche Médicale (ECO20160736105).

REFERENCES

Aoki, Y. et al., 2003. Sox10 regulates the development of neural crest-derived melanocytes in Xenopus. *Developmental Biology*, 259(1), pp.19–33.

Bailey, A.P. et al., 2006. Lens specification is the ground state of all sensory placodes, from which FGF promotes olfactory identity. *Developmental cell*, 11(4), pp.505–517.

Basch, M.L., Bronner-Fraser, M. & Garcia-Castro, M.I., 2006. Specification of the neural crest occurs during gastrulation and requires Pax7. *Nature*, 441(7090), pp.218–222.

bioRxiv preprint doi: https://doi.org/10.1101/168807; this version posted July 26, 2017. The copyright holder for this preprint (which was not certified by peer review) is the author/funder. All rights reserved. No reuse allowed without permission.

544 Bellmeyer, A. et al., 2003. The Protooncogene c-Myc Is an Essential Regulator of Neural Crest
545 Formation in Xenopus. *Developmental Cell*, 4(6), pp.827–839.
546 Betancur, P. et al., 2014. Expression and function of transcription factor cMyb during cranial neural
547 crest development. *Mechanisms of Development*, 132(1), pp.38–43.
548 Betancur, P., Bronner-fraser, M. & Sauka-Spengler, T., 2010. Assembling Neural Crest Regulatory
549 Circuits into a Gene Regulatory Network. *Annual Review in Cell and Developmental Biology,* 26,
550 pp.581-603
551 Blum, M. et al., 2015. Morpholinos: Antisense and Sensibility. *Developmental cell*, 35(2), pp.145–149.
552 Bradley, R.S., Espeseth, A. & Kintner, C., 1998. NF-protocadherin, a novel member of the cadherin
553 superfamily, is required for Xenopus ectodermal differentiation. *Current biology : CB*, 8(6), pp.325–
554 334.
555 Brewer, S. et al., 2004. Wnt1-Cre-mediated deletion of AP-2alpha causes multiple neural crest-related
556 defects. *Developmental biology*, 267(1), pp.135–152.
557 Bronner, M.E. & LeDouarin, N.M., 2012. Development and evolution of the neural crest: An overview.
558 *Developmental Biology*, 366(1), pp.2–9.
559 Carballada, R., Yasuo, H. & Lemaire, P., 2001. Phosphatidylinositol-3 kinase acts in parallel to the
560 ERK MAP kinase in the FGF pathway during Xenopus mesoderm induction. *Development*, 128,
561 pp.35–44.
562 Chang, C. & Hemmati-Brivanlou, A., 1998. Neural crest induction by Xwnt7B in Xenopus.
563 *Developmental biology*, 194(1), pp.129–134.
564 Courtnay, R. et al., 2015. Cancer metabolism and the Warburg effect: the role of HIF-1 and PI3K.
565 *Molecular biology reports*, 42(4), pp.841–851.
566 de Crozé, N., Maczkowiak, F. & Monsoro-Burq, A.H., 2011. Reiterative AP2a activity controls
567 sequential steps in the neural crest gene regulatory network. *Proceedings of the National Academy*
568 *of Sciences of the United States of America*, 108(1), pp.155–60.
569 Datta, S.R., Brunet, A. & Greenberg, M.E., 1999. Cellular survival: a play in three Akts. *Genes &*
570 *development*, 13(22), pp.2905–2927.
571 Douarin, N.L. & Kalcheim, C., 1999. *The Neural Crest*, Cambridge University Press.
572 Essex, L.J., Mayor, R. & Sargent, M.G., 1993. Expression of Xenopus snail in mesoderm and
573 prospective neural fold ectoderm. *Developmental dynamics* 198(2), pp.108–122.
574 Fu, Q.-F. et al., 2015. Alpha-enolase promotes cell glycolysis, growth, migration, and invasion in non-
575 small cell lung cancer through FAK-mediated PI3K/AKT pathway. *Journal of hematology &*
576 *oncology*, 8 : 22.

bioRxiv preprint doi: https://doi.org/10.1101/168807; this version posted July 26, 2017. The copyright holder for this preprint (which was not certified by peer review) is the author/funder. All rights reserved. No reuse allowed without permission.

577 Gammill, L.S. & Sive, H., 2000. Coincidence of otx2 and BMP4 signaling correlates with Xenopus
578 cement gland formation. *Mechanisms of development*, 92(2), pp.217–226.
579 Graff, J.M. et al., 1994. Studies with a Xenopus BMP receptor suggest that ventral mesoderm-
580 inducing signals override dorsal signals in vivo. *Cell*, 79(1), pp.169–179.
581 Grammer, T.C. et al., 2000. Use of large-scale expression cloning screens in the Xenopus laevis
582 tadpole to identify gene function. *Developmental biology*, 228(2), pp.197–210.
583 Han, T. et al., 2013. How does cancer cell metabolism affect tumor migration and invasion? *Cell*
584 *adhesion & migration*, 7(5), pp.395–403.
585 Heasman, J., Kofron, M. & Wylie, C., 2000. Beta-catenin signaling activity dissected in the early
586 Xenopus embryo: a novel antisense approach. *Developmental biology*, 222(1), pp.124–134.
587 Heike, C.L., Luquetti, D. V & Hing, A. V, 1993. Craniofacial Microsomia Overview. In R. A. Pagon et
588 al., eds. Seattle (WA).
589 Hirschhaeuser, F., Sattler, U.G.A. & Mueller-Klieser, W., 2011. Lactate: a metabolic key player in
590 cancer. *Cancer research*, 71(22), pp.6921–6925.
591 Hopwood, N.D., Pluck, A. & Gurdon, J.B., 1989a. A Xenopus mRNA related to Drosophila twist is
592 expressed in response to induction in the mesoderm and the neural crest. *Cell*, 59(5), pp.893–
593 903.
594 Hopwood, N.D., Pluck, A. & Gurdon, J.B., 1989b. MyoD expression in the forming somites is an early
595 response to mesoderm induction in Xenopus embryos. *The EMBO journal*, 8(11), pp.3409–3417.
596 Hu, N. et al., 2012. DNA methyltransferase3A as a molecular switch mediating the neural tube-to-
597 neural crest fate transition. *Genes & development*, 26(21), pp.2380–5.
598 Ito, K. & Suda, T., 2014. Metabolic requirements for the maintenance of self-renewing stem cells.
599 *Nature reviews. Molecular cell biology*, 15(4), pp.243–256.
600 Khadka, D., Luo, T. & Sargent, T.D., 2006. Msx1 and Msx2 have shared essential functions in neural
601 crest but may be dispensable in epidermis and axis formation in Xenopus. *The International journal*
602 *of developmental biology*, 50(5), pp.499–502.
603 LaBonne, C. & Bronner-Fraser, M., 1998. Neural crest induction in Xenopus: evidence for a two-
604 signal model. *Development* , 125(13), pp.2403–14.
605 Lamb, T.M. et al., 1993. Neural induction by the secreted polypeptide noggin. *Science*, 262(5134),
606 pp.713–718.
607 Lander, R. et al., 2013. Interactions between Twist and other core epithelial-mesenchymal transition
608 factors are controlled by GSK3-mediated phosphorylation. *Nature communications*, 4 : 1542.
609 Leevers, S.J., Vanhaesebroeck, B. & Waterfield, M.D., 1999. Signalling through phosphoinositide 3-
610 kinases: the lipids take centre stage. *Current opinion in cell biology*, 11(2), pp.219–225.

bioRxiv preprint doi: https://doi.org/10.1101/168807; this version posted July 26, 2017. The copyright holder for this preprint (which was not certified by peer review) is the author/funder. All rights reserved. No reuse allowed without permission.

611 Li, B. et al., 2009. The posteriorizing gene Gbx2 is a direct target of Wnt signalling and the earliest
612 factor in neural crest induction. *Development*, 136(19), pp.3267–78.
613 Lincet, H. & Icard, P., 2015. How do glycolytic enzymes favour cancer cell proliferation by
614 nonmetabolic functions? *Oncogene*, 34(29), pp.3751–3759.
615 Luo, T. et al., 2003. Induction of neural crest in Xenopus by transcription factor AP2alpha.
616 *Proceedings of the National Academy of Sciences of the United States of America*, 100(2),
617 pp.532–537.
618 Lwigale, P.Y., 2015. Corneal Development: Different Cells from a Common Progenitor. *Progress in*
619 *molecular biology and translational science*, 134, pp.43–59.
620 Maczkowiak, F. et al., 2010. The Pax3 and Pax7 paralogs cooperate in neural and neural crest
621 patterning using distinct molecular mechanisms, in Xenopus laevis embryos. *Developmental*
622 *biology*, 340(2), pp.381–96.
623 Manning, B.D. & Cantley, L.C., 2007. AKT/PKB signaling: navigating downstream. *Cell*, 129(7),
624 pp.1261–1274.
625 Mayor, R., Morgan, R. & Sargent, M.G., 1995. Induction of the prospective neural crest of Xenopus.
626 *Development*, 121(3), pp.767–777.
627 Meulemans, D. & Bronner-Fraser, M., 2004. Gene-regulatory interactions in neural crest evolution
628 and development. *Developmental Cell*, 7(3), pp.291–299.
629 Milet, C. et al., 2013. Pax3 and Zic1 drive induction and differentiation of multipotent, migratory, and
630 functional neural crest in Xenopus embryos. *Proceedings of the National Academy of Sciences of*
631 *the United States of America*, 110(14), pp.5528–33.
632 Milet, C. & Monsoro-Burq, A.H., 2014. Dissection of Xenopus laevis neural crest for in vitro explant
633 culture or in vivo transplantation. *Journal of visualized experiments : JoVE*, (85), p.e51118.
634 Available at: http://www.jove.com/video/51118/dissection-xenopus-laevis-neural-crest-for-vitro-
635 explant-culture-or .
636 Milet, C. & Monsoro-Burq, A.H., 2012. Neural crest induction at the neural plate border in vertebrates.
637 *Developmental biology*, 366(1), pp.22–33.
638 Mizuseki, K. et al., 1998. Xenopus Zic-related-1 and Sox-2, two factors induced by chordin, have
639 distinct activities in the initiation of neural induction. *Development*, 125(4), pp.579–587.
640 Monsoro-Burq, A.-H., Fletcher, R.B. & Harland, R., 2003. Neural crest induction by paraxial
641 mesoderm in Xenopus embryos requires FGF signals. *Development*, 130(14), pp.3111–3124.
642 Monsoro-Burq, A.-H., Wang, E. & Harland, R., 2005. Msx1 and Pax3 cooperate to mediate FGF8 and
643 WNT signals during Xenopus neural crest induction. *Developmental cell*, 8(2), pp.167–78.

bioRxiv preprint doi: https://doi.org/10.1101/168807; this version posted July 26, 2017. The copyright holder for this preprint (which was not certified by peer review) is the author/funder. All rights reserved. No reuse allowed without permission.

644 Monsoro-Burq, A.H., 2007. A rapid protocol for whole-mount in situ hybridization on Xenopus
645 embryos. *CSH protocols*, 2007, p.pdb.prot4809.
646 Neave, B., Holder, N. & Patient, R., 1997. A graded response to BMP-4 spatially coordinates
647 patterning of the mesoderm and ectoderm in the zebrafish. *Mechanisms of development*, 62(2),
648 pp.183–195.
649 Nichane, M. et al., 2008. Hairy2-Id3 interactions play an essential role in Xenopus neural crest
650 progenitor specification. *Developmental biology*, 322(2), pp.355–67.
651 Nieto, M.A. et al., 1994. Control of cell behavior during vertebrate development by Slug, a zinc finger
652 gene. *Science*, 264(5160), pp.835–839.
653 Nieuwkoop, P.D. & Faber, J., 1994. *Normal Table of Xenopus Laevis (Daudin): A Systematical and*
654 *Chronological Survey of the Development from the Fertilized Egg Till the End of Metamorphosis*,
655 Garland Pub.
656 Okar, D. a et al., 2001. PFK-2/FBPase-2:maker and breaker of the essential biofactor fructose-2, 6-
657 bisphosphate. *Trends in biochemical sciences*, 26(1).
658 Pegoraro, C. et al., 2015. PFKFB4 controls embryonic patterning via Akt signalling independently of
659 glycolysis. *, Nat Commun.* 6:5953. doi: 10.1038/ncomms6953
660
661 Pegoraro, C., MacZkowiak, F. & Monsoro-Burq, A.H., 2013. Pfkfb (6-phosphofructo-2-kinase/fructose-
662 2,6-bisphosphatase) isoforms display a tissue-specific and dynamic expression during Xenopus
663 laevis development. *Gene Expression Patterns*, 13(7), pp.203–211.
664 Pegoraro, C. & Monsoro-Burq, A.H., 2012. Signaling and transcriptional regulation in neural crest
665 specification and migration: lessons from xenopus embryos. *Developmental biology*, 2(2), pp.247–
666 59.
667 Peng, Y. et al., 2004. Phosphatidylinositol 3-kinase signaling is involved in neurogenesis during
668 Xenopus embryonic development. *The Journal of biological chemistry*, 279(27), pp.28509–14.
669 Peyssonnaux, C. et al., 2000. Induction of postmitotic neuroretina cell proliferation by distinct Ras
670 downstream signaling pathways. *Molecular and cellular biology*, 20(19), pp.7068–7079.
671 Pilkis, S.J., Claus, T.H. & Kurland, I., 1995. 6-Phoshphofructo-2-kinase/Fructose-2,6-bisphosphatase:
672 a metabolic signaling enzyme. *Annual Review of Biochemistry*, 64, pp.799–835.
673 Plouhinec, J.-L. et al., 2014. Pax3 and Zic1 trigger the early neural crest gene regulatory network by
674 the direct activation of multiple key neural crest specifiers. *Developmental biology*, 386(2), pp.461–
675 72.

bioRxiv preprint doi: https://doi.org/10.1101/168807; this version posted July 26, 2017. The copyright holder for this preprint (which was not certified by peer review) is the author/funder. All rights reserved. No reuse allowed without permission.

676 Qu, J. et al., 2016. PFKFB3 modulates glycolytic metabolism and alleviates endoplasmic reticulum
677 stress in human osteoarthritis cartilage. *Clinical and experimental pharmacology & physiology*,
678 43(3), pp.312–318.
679 Saint-Jeannet, J.P. et al., 1989. Expression of N-CAM precedes neural induction in Pleurodeles waltl
680 (urodele, amphibian). *Development*, 106(4), pp.675–683.
681 Saint-Jeannet, J.P. et al., 1997. Regulation of dorsal fate in the neuraxis by Wnt-1 and Wnt-3a.
682 *Proceedings of the National Academy of Sciences of the United States of America*, 94(25),
683 pp.13713–13718.
684 Sato, T., Sasai, N. & Sasai, Y., 2005. Neural crest determination by co-activation of Pax3 and Zic1
685 genes in Xenopus ectoderm. *Development*, 132(10), pp.2355–63.
686 Scheel, C. & Weinberg, R.A., 2012. Cancer stem cells and epithelial-mesenchymal transition:
687 concepts and molecular links. *Seminars in cancer biology*, 22(5-6), pp.396–403.
688 Sharpe, P.T. et al., 1988. Isolation and expression of a new mouse homeobox gene. *Development*,
689 102(2), pp.397–407.
690 Simões-Costa, M. et al., 2014. Transcriptome analysis reveals novel players in the cranial neural
691 crest gene regulatory network. *Genome research*, 24(2), pp.281–90.
692 Simões-Costa, M., Stone, M. & Bronner, M.E., 2015. Axud1 Integrates Wnt Signaling and
693 Transcriptional Inputs to Drive Neural Crest Formation. *Developmental cell*, 34(5), pp.544–554.
694 Sive, H.L., Grainger, R.M. & Harland, R.M., 2010. *Early Development of Xenopus Laevis: A*
695 *Laboratory Manual*, Cold Spring Harbor Laboratory Press. Available at:
696 https://books.google.pt/books?id=ULDpRAAACAAJ.
697 Spokony, R.F. et al., 2002. The transcription factor Sox9 is required for cranial neural crest
698 development in Xenopus. *Development*, 129(2), pp.421–432.
699 Steventon, B. et al., 2009. Differential requirements of BMP and Wnt signalling during gastrulation
700 and neurulation define two steps in neural crest induction. *Development*, 136(5), pp.771–9.
701 Strobl-Mazzulla, P.H., Sauka-Spengler, T. & Bronner-Fraser, M., 2010. Histone demethylase JmjD2A
702 regulates neural crest specification. *Developmental cell*, 19(3), pp.460–8.
703 Théveneau, E., Duband, J.L. & Altabef, M., 2007. Ets-1 confers cranial features on neural crést
704 delamination. *PLoS ONE*, 2(11).
705 Theveneau, E. & Mayor, R., 2012. Neural crest delamination and migration: from epithelium-to-
706 mesenchyme transition to collective cell migration. *Developmental biology*, 366(1), pp.34–54.
707 Trefely, S. et al., 2015. Kinome Screen Identifies PFKFB3 and Glucose Metabolism as Important
708 Regulators of the Insulin/Insulin-like Growth Factor (IGF)-1 Signaling Pathway. *The Journal of*
709 *biological chemistry*, 290(43), pp.25834–25846.

bioRxiv preprint doi: https://doi.org/10.1101/168807; this version posted July 26, 2017. The copyright holder for this preprint (which was not certified by peer review) is the author/funder. All rights reserved. No reuse allowed without permission.

Tsien, R.Y., 1998. The green fluorescent protein. *Annual review of biochemistry*, 67, pp.509–544.

Valluet, A. et al., 2012. B-Raf and C-Raf are required for melanocyte stem cell self-maintenance. *Cell reports*, 2(4), pp.774–80.

Vega, S. et al., 2004. Snail blocks the cell cycle and confers resistance to cell death. *Genes and Development*, 18, pp. 1131-1143

Villanueva, S. et al., 2002. Posteriorization by FGF, Wnt, and retinoic acid is required for neural crest induction. *Developmental biology*, 241(2), pp.289–301.

Wilson, N.R. et al., 2016. SPECC1L deficiency results in increased adherens junction stability and reduced cranial neural crest cell delamination. *Scientific reports*, 6, p.17735.

Wilson, P.A. et al., 1997. Concentration-dependent patterning of the Xenopus ectoderm by BMP4 and its signal transducer Smad1. *Development*, 124(16), pp.3177–3184.

Yalcin, A. et al., 2009. Nuclear targeting of 6-phosphofructo-2-kinase (PFKFB3) increases proliferation via cyclin-dependent kinases. *Journal of Biological Chemistry*, 284(36), pp.24223–24232.

Yang, W. et al., 2011. Nuclear PKM2 regulates β-catenin transactivation upon EGFR activation. *Nature*, 478(7375), pp.118–122.

Yang, W. et al., 2012. PKM2 phosphorylates histone H3 and promotes gene transcription and tumorigenesis. *Cell*, 150(4), pp.685–696.

FIGURE LEGENDS

Fig. 1. PFKFB4 promotes neural border and neural crest formation.

(A) NC is induced during neural plate stage (st.12.5 to st.14). NB specifiers expression (red) is robustly established lateral to the neural plate, early NC specifiers expression (*snail2, foxd3)* is faintly initiated (light pink). (B-C) During neural fold elevation (st.14 to st.17), future NC cells progressively acquire their definitive specification and specific cellular properties (survival, expression of late NC specifiers, cadherin switch...) ensuring their ability to undergo EMT and migration at the end of neurulation (C, st.18 to st.19). (D-F,H,I) *Pfkfb4* is enriched in the NB/NC in neurulas and tadpoles. (J) *Pfkfb3* is expressed in the neural tube. Sense probes (*pfkfb4*, G; *pfkfb3*, K). Neurula stages: late gastrula/early neural plate stage: st.12 (D), end of neural plate stage, st.14 (E), neural fold stage; st.16 (F), neural tube closure/ end of neurulation: st.19 (H). Tailbud stage: st.22 (I). E-H, J,K: dorsal views, anterior to the right. D,I: side views. Scale bar, 1mm. (L-N) Cross-sections through the mid-neurula anterior neural plate (st.14) show *snail2* and *pfkfb4* expression in NB/NC. (L) The notochord, neural plate and paraxial mesoderm are outlined on hematoxylin-eosin stained sections. (M-N)

bioRxiv preprint doi: https://doi.org/10.1101/168807; this version posted July 26, 2017. The copyright holder for this preprint (which was not certified by peer review) is the author/funder. All rights reserved. No reuse allowed without permission.

744 Vibratome sections. Arrow indicates the midline. Arrowheads indicate the st.14 NB (red bar). Scale
745 bar, 200μm. (O-S) *pfkfb4* gain-of-function expanded the st.14 NB (O,P, 59% of embryos with enlarged
746 NB compared to the contralateral uninjected side, n=81) and premigratory NC (Q, st.14, 59%
747 enlarged *Snail2* expression, n=147), (R,S: st.18, 55% increase, n=271). Migrating NC streams were
748 expanded (T,Z, st. 22-24, 65% expansion, n=49). In contrast, pan- or regional neural plate markers
749 (*sox2*, *otx2, hoxb9*), ectoderm (*keratin K81, ep.Ker.*) or paraxial mesoderm (*myod*) markers were
750 unaffected (U-Y). O-S, U-X: dorsal views. T,Z: side views, Y: dorsal-posterior view. Scale bar=500μm.
751 Detailed phenotype scoring in Table.S2.

752

753 **Fig. 2. Moderate PFKFB4 depletion results in severe craniofacial defects in tadpoles.**
754 (A) *Pfkfb4* mRNA levels were quantified on neurulas dorsal tissues (RTqPCR). Injections at "high
755 concentration" (10ng/cell in 4-cell-stage embryos) reduced *pfkfb4* levels by 52% and caused
756 developmental arrest. "Milder" concentration (5ng/cell in 4-cell-stage embryos) decreased *pfkfb4*
757 mRNA by 32% (low-level depletion), and allowed swimming tadpoles development. (B-E) Craniofacial
758 morphology in tadpoles st.45-46. Low-level PFKFB4MO depletion reduced craniofacial structures on
759 the injected side (n=17). The branchial arch cartilages area was severely diminished on the injected
760 side (36% reduction compared to the contralateral side, n=8; p-value<0.0001 compared to side-to-
761 side variations in a control population, n=9). Lower doses did not significantly reduce cartilage area
762 (n= 6), or affect head morphology (n=20). (C) Head morphology, dorsal view, arrowhead: injected
763 side. (D) Dissected jaw and branchial arches cartilages, ventral view, arrowheads: injected side. (E)
764 Scheme of D. Scale bar,500 μm.

765

766 **Fig. 3. PFKFB4 low-level depletion delays NC early specification, causes retention of NB**
767 **character, impairs NC late specification and migration.**
768 (A) At st.14, *snail2* expression was severely reduced, or abolished, on the injected side (reduced in
769 78% of embryos, n=42*).* (B) At st.18, sibling embryos had recovered *snail2* expression (normal in
770 73% of embryos, n=66). (C-D) While *sox10* expression was mainly unaffected (65%, n=31), *twist* was
771 severely impaired (65%, n=49). (E-H) In contrast, expression of the immature NC marker *hes4* was
772 expanded (73%, n=37), as were some NB markers, either strongly (*pax3*, 100%, n=39) or moderately
773 (*zic1*, 46% n=13). Other NB markers were unperturbed (*msx1,* normal in 80% of embryos, n=10). (I-K)
774 Neural plate (*sox2*, n=13), non-neural ectoderm (*ep.ker*., n=12) and paraxial mesoderm (*myod,* n=4)
775 seemed unaffected. (L) Percent of embryos with each phenotype, details in Table.S2. A-K: dorsal
776 views. (M-R) St.24 tailbud embryos exhibited a severe NC migration defect (M-Q, *sox10,* 50%, n=10;

bioRxiv preprint doi: https://doi.org/10.1101/168807; this version posted July 26, 2017. The copyright holder for this preprint (which was not certified by peer review) is the author/funder. All rights reserved. No reuse allowed without permission.

twist 56%, n=25). *Sox2* expression appeared grossly unaffected, despite marginal reduction of optic vesicle size (R, n=5). (S) Co-injection of *pfkfb4* mRNA with PFKFBMO rescued both *sox10*/*twist* alterations of expression and NC migration defects in a significant proportion of the embryos, compared to PFKFB4MO injections: *sox10* and *twist* expression were restored or increased a majority of the embryos (n=29 and n=18 respectively). The injected side (inj) is compared to the control side (co) in side views (M,N,P,Q, anterior to the right) or frontal views (O, R, red arrow on injected side). Scale bar, 500 μm.

Fig. 4. Inducible depletion demonstrates independent PFKFB4 roles in NC specification and migration. We co-injected a UV-cleavable sense MO (PhMO) to block PFKFB4MO until the desired developmental stage and monitored *twist* expression at st18. (A-H) Strategy of phMO validation: *lacZ* control injections (A), unmasked PFKFB4MO, "high" dose (B), PhMO/MO without UV illumination (C, uninduced, u.i); UV illumination at early NC specification st12.5 (D-G). (A) *LacZ* injections did not alter *twist* pattern (100%, n=31). PFKFB4MO severely blocked *twist* expression (abolished (80%) or diminished (17%) n=35). *Twist* decreased in PhMO/MO-injected embryos UV-illuminated immediately after injection (a.i.) (H, 73%, n=15). *Pfkfb4* depletion, activated at st12.5, decreased *twist* expression strongly (47%), or moderately (22.6%) (n=53). This effect persisted until EMT and early NC emigration (G, stage 20). (A-G): dorsal views. (I-W) To deplete *pfkfb4* during EMT/early migration, st. 18 neurulas were UV illuminated and analyzed at tadpole st 24. *Twist* was normal in embryos injected with *lacZ* (I,J; n=41), or with PhMO/MO but not illuminated (M,N; n=38). Cells injected with PFKFB4MO alone died as expected (K,L; n=52). PhMO/MO-injected embryos UV-illuminated at st. 18 exhibited three phenotypes classes (n=42): "migration" (O,P), "staining and migration" (Q,R) and "severe staining" defects (S,T). We compared percent of each phenotype (U), percent of migration distance (V), percent of NC stream area (W, *twist*-expressing area) to the contralateral side. Scale bars = 500 μm. All phenotype differences were statistically significant between illuminated PhMO/MO-injected embryos, and either *lacZ*-injected, or uninduced PhMO/MO-injected embryos (*: p-value<0.05; **: p-value<0.01; ***: p-value<0.001; ns: non significant).

Fig. 5: AKT signaling mediates PFKFB4 function on premigratory NC maturation.

(A) In embryos, PFKFB4 can regulate AKT signaling in addition to glycolysis rate. Here, in morphants, dissected st. 14 NB or st. 17 NC displayed decreased activated AKT signaling levels. (B) AKT regulates many aspects of cell homeostasis including cell proliferation, cell survival, and cell metabolism. Here, embryos injected with *gfp* and MO in NC area were selected and sectioned: cell counting after EdU incorporation showed that cell proliferation rate was normal after PFKFB4MO

bioRxiv preprint doi: https://doi.org/10.1101/168807; this version posted July 26, 2017. The copyright holder for this preprint (which was not certified by peer review) is the author/funder. All rights reserved. No reuse allowed without permission.

injections. (C, D) PFKFB4MO affected late NC specifier *twist* expression, while NC stem cells marker *cmyc* was normally activated. (E-H) Pharmacological treatment during neural fold stage (st. 14 to st. 18) showed that blocking MAPK signaling (E, G) did not affect NC development, while blocking PI3K-AKT signaling (F, H) affected *twist* but not *cmyc*, thus phenocopying PFKFB4MO effect. (I, J) Coinjection of PFKFB4MO with a constitutively AKT (blue arrows) rescued the morphant *twist* phenotype (red arrows): two sibling embryos for each injection are shown. St. 18 *pfkfb4* morphants presented diminished *twist* (69%, n=26). (B) In contrast, siblings co-injected with PFKFB4MO and *caAkt* mRNA had normal *twist* expression in the majority of cases (73% normal or enlarged, n=42). Scale bars = 500 μm.

Fig. 6. PFKFB4 morphant neural crest progenitors fail to undergo EMT and migration.
(A, B) When transplanted into a wild-type host embryo, GFP-labeled wild-type NC efficiently migrates and populates the host branchial arches, whichever the size of the grafted tissue (A) large graft, (B) small graft (20/24 cases, n=24). (C, D) In contrast, PFKFB4 morphant NC exhibited defective healing, resulting in small-size grafts, which yielded few, if any, migratory NCC into the host craniofacial area (n=23, occasional migration in 9/23 grafted embryos). (C) Small graft without migratory cells and (D) small graft with few cells reaching the branchial arches, *gfp* staining by WISH to enhance individual cell visualisation. (E) *N-cadherin* expression (RTqPCR on dissected explants), either prior to EMT (NB, st. 14), or in premigratory NC (st. 17). (F-J) Wild-type or morphant cells were lineage traced *in vivo*, on embryos injected in the prospective neural fold unilaterally (F, H). (G-J) At tailbud stage, control cells (G) efficiently populated branchial arches and were also found in brain and eye (J). In contrast, morphant cells failed to populate branchial arches (I) in a dose-dependent manner (J), but were normally found in the brain and eye (J). (K-R) NB were dissected prior to EMT (st. 14), plated onto fibronectin. Cell behavior was followed by time-lapse videomicroscopy. Wild-type NC (K-N) adheres efficiently, undergoes EMT (L), cell scattering and migration (M, N). Morphant NC (O-R) presented poor adherence, delayed (P) and inefficient EMT (Q), and few emigrating cells (R). Scale bar = 160 μm.

Fig. 7. Glycolysis and PI3K-AKT signaling impact NC migration similarly to PFKFB4 low-level depletion, and activating AKT signaling rescues PFKFB4 downregulation.
(A-H) When glycolysis (2DG) or PI3K-AKT pathway (LY294002) were blocked during EMT and migration (st. 18 to st. 24) both treatments severely affected NC migration at st. 24 (*twist*, n=16 (2DG), n=14 (LY); s*ox10* (n= 11 (2DG), n=12 (LY). (I-L) At st. 45, tadpoles treated during NC migration then grown in control medium, exhibited general head morphology defects, including eye defects and

bioRxiv preprint doi: https://doi.org/10.1101/168807; this version posted July 26, 2017. The copyright holder for this preprint (which was not certified by peer review) is the author/funder. All rights reserved. No reuse allowed without permission.

reduced branchial cartilages. (I, K) sibling controls, n=30; (J) 2DG, n=13; (L) LY294002, n=19. (A-H) side views, (I-L) dorsal view. (M) At tadpole st. 45, morphant sides were severely affected (P, 83% embryos with craniofacial reduction, n=23), while activation of *Akt* signaling (N) did not affect overall craniofacial morphogenesis (P, 92% symmetrical, n=59). Tadpoles co-injected with PFKFB4MO and *caAkt* (O) were largely rescued, with 66% of embryos with injected side symmetrical to contralateral side (P, n=63). (M) Red bar: eye distance from the midline (morphant side). Blue bar: control distance. Both bars were aligned for comparison. (N) On both sides, the same blue bar measures eye distance from the midline. Scale bar = 500 μm.

Fig. 8. *Pfkfb4* activation during neural fold stage is regulated by the neural crest GRN.
(A-Y) Unilateral depletion of members of the NC-GRN modulated *pfkfb4* activation at the NB (st.14) and NC (st.18). (A-H) Blockade of WNT and FGF signaling strongly decreased *snail2* and *pfkfb4* expression. (I-L). Conversely, BMP signaling downregulation upregulated *snail2* and *pfkfb4* expression, laterally to the NB. (M-T) Knockdown of the NC specifiers PAX3 and TFAP2a resulted in loss of *snail2* and *pfkfb4*. (U-Y) Knockdown of the NC specifier SOX9 depleted *snail2* and *pfkfb4*. Dorsal views, injected side on the right. Detailed scoring: see Table S2. Scale bar = 500μm.

Fig. 9. Model of PFKFB4-controlled AKT signaling in NC maturation, EMT and migration.
During neurulation, in control conditions (left side), NC induction is initiated at the neural plate stage with weak *snail2* expression. This initial induction is then strengthened during neural fold stage, under the action of the NC-GRN which, in particular, activates *pfkfb4* expression in NC progenitors. This second phase allows acquisition of cellular ability to undergo EMT and migration upon neural tube closure. When AKT signaling is defective (right side), either after PFKFB4 low-level depletion, or using pharmacological inhibitors, delays in NC specification cascade occur, incomplete maturation is observed, and NC fails to undergo EMT. When PFKFB4 and AKT functions are prevented after EMT, fewer NC cell migrate. As a result, reduced craniofacial skeletal elements form. This series of results shows that the steps of NC early development rely upon a continuous and elevated AKT signaling level, sustained by PFKFB4, itself triggered by the NC-GRN.

bioRxiv preprint doi: https://doi.org/10.1101/168807; this version posted July 26, 2017. The copyright holder for this preprint (which was not certified by peer review) is the author/funder. All rights reserved. No reuse allowed without permission.

Fig.1

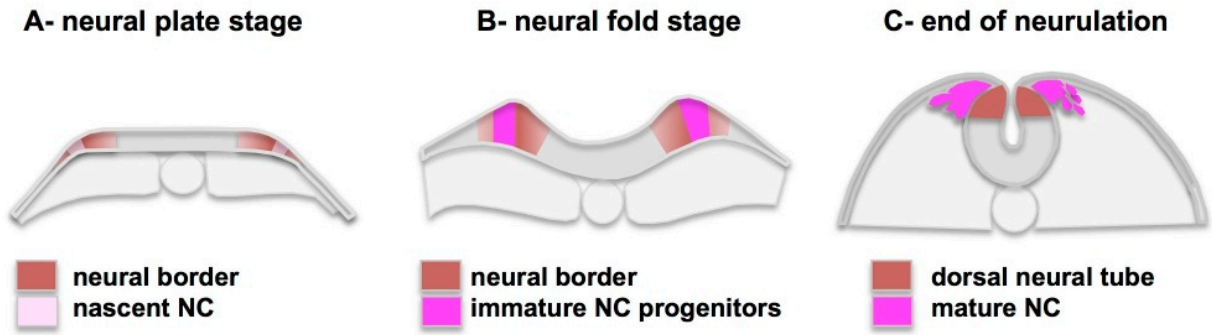

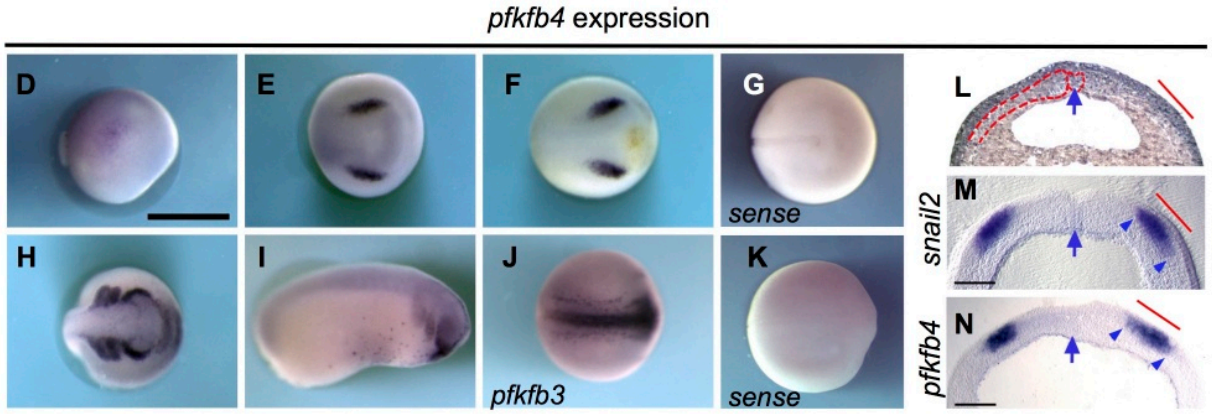

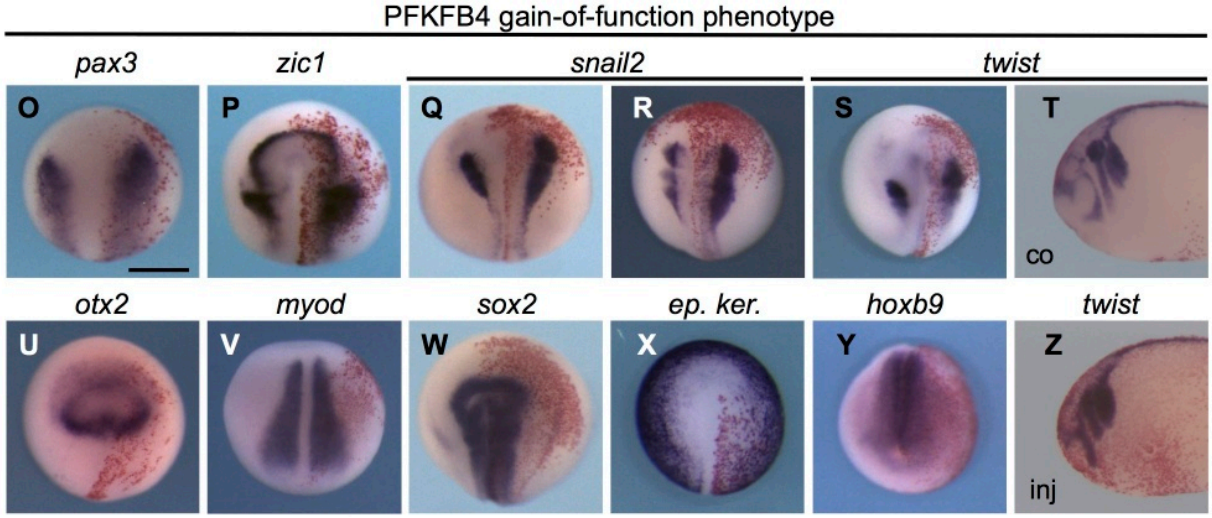

bioRxiv preprint doi: https://doi.org/10.1101/168807; this version posted July 26, 2017. The copyright holder for this preprint (which was not certified by peer review) is the author/funder. All rights reserved. No reuse allowed without permission.

Fig. 2

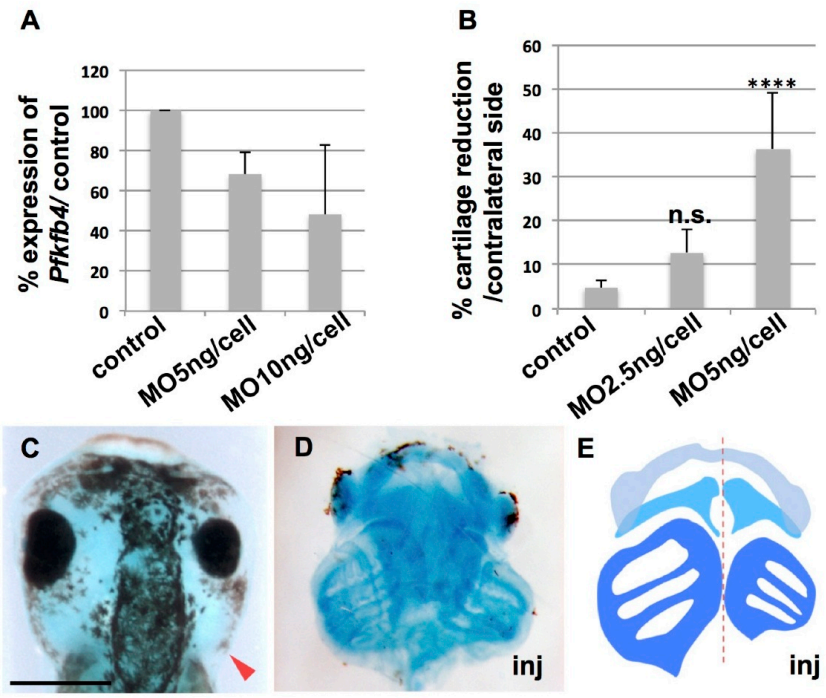

bioRxiv preprint doi: https://doi.org/10.1101/168807; this version posted July 26, 2017. The copyright holder for this preprint (which was not certified by peer review) is the author/funder. All rights reserved. No reuse allowed without permission.

Fig. 3

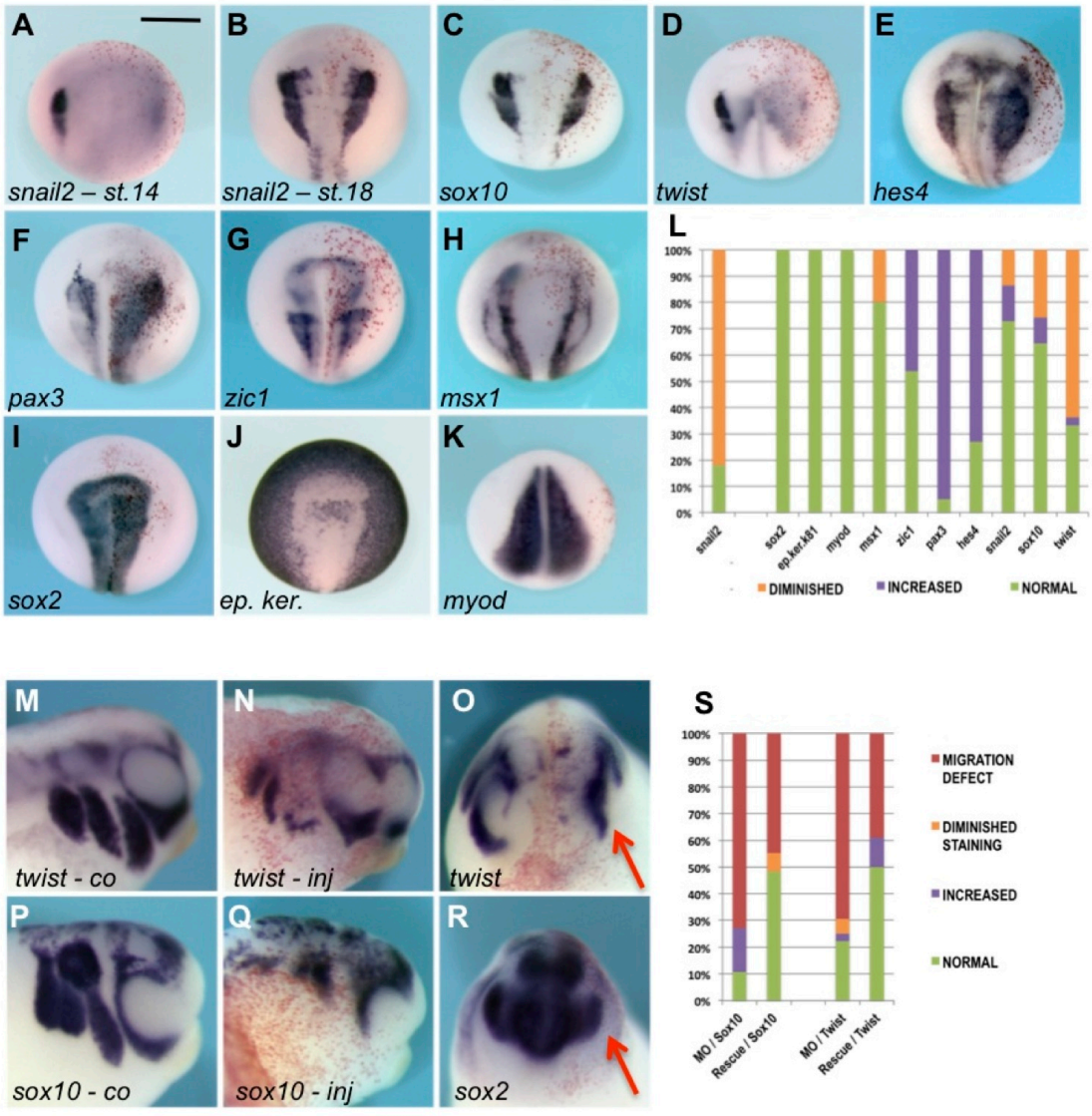

bioRxiv preprint doi: https://doi.org/10.1101/168807; this version posted July 26, 2017. The copyright holder for this preprint (which was not certified by peer review) is the author/funder. All rights reserved. No reuse allowed without permission.

Fig. 4

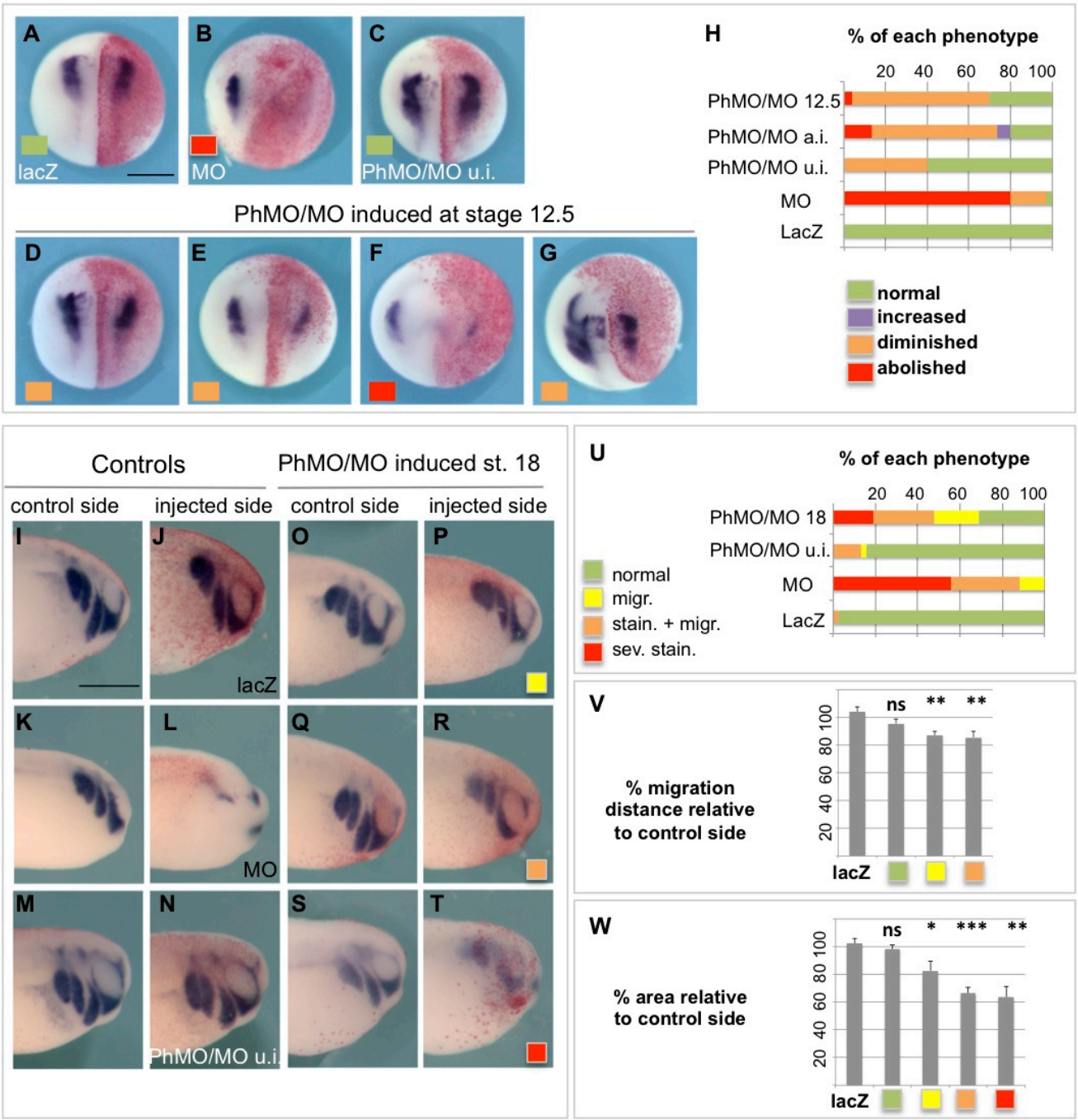

bioRxiv preprint doi: https://doi.org/10.1101/168807; this version posted July 26, 2017. The copyright holder for this preprint (which was not certified by peer review) is the author/funder. All rights reserved. No reuse allowed without permission.

Fig. 5

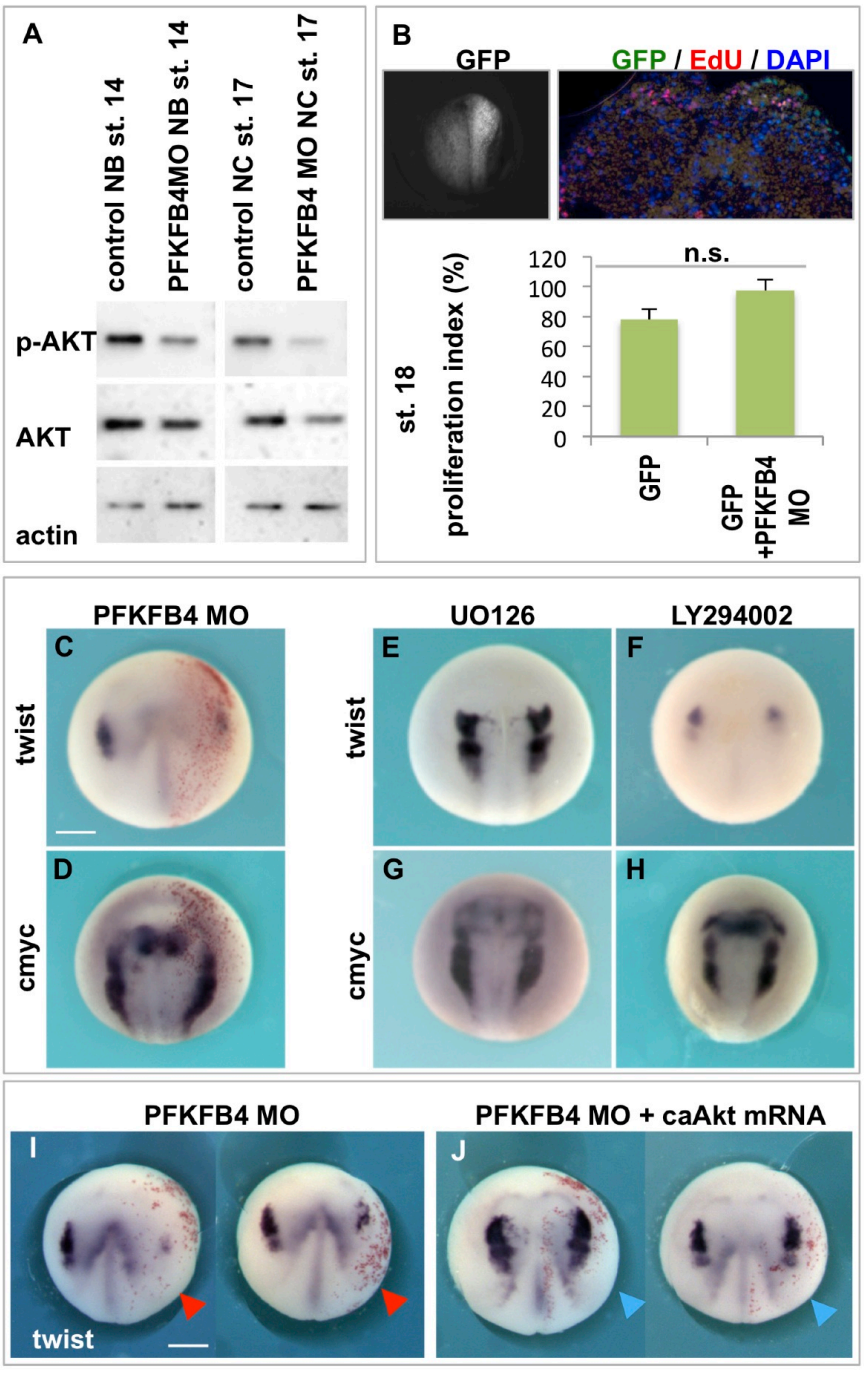

bioRxiv preprint doi: https://doi.org/10.1101/168807; this version posted July 26, 2017. The copyright holder for this preprint (which was not certified by peer review) is the author/funder. All rights reserved. No reuse allowed without permission.

Fig. 6

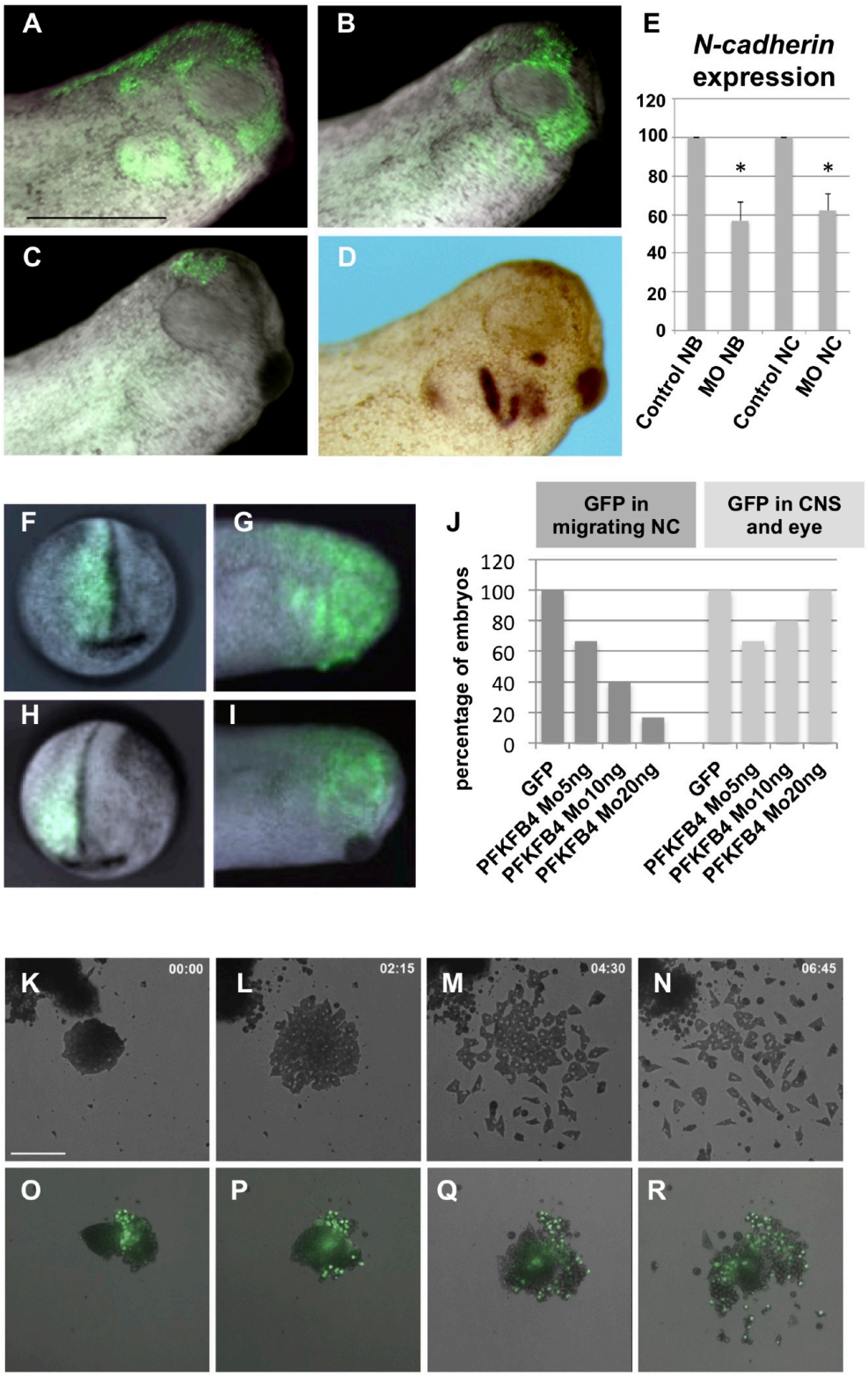

bioRxiv preprint doi: https://doi.org/10.1101/168807; this version posted July 26, 2017. The copyright holder for this preprint (which was not certified by peer review) is the author/funder. All rights reserved. No reuse allowed without permission.

Fig. 7

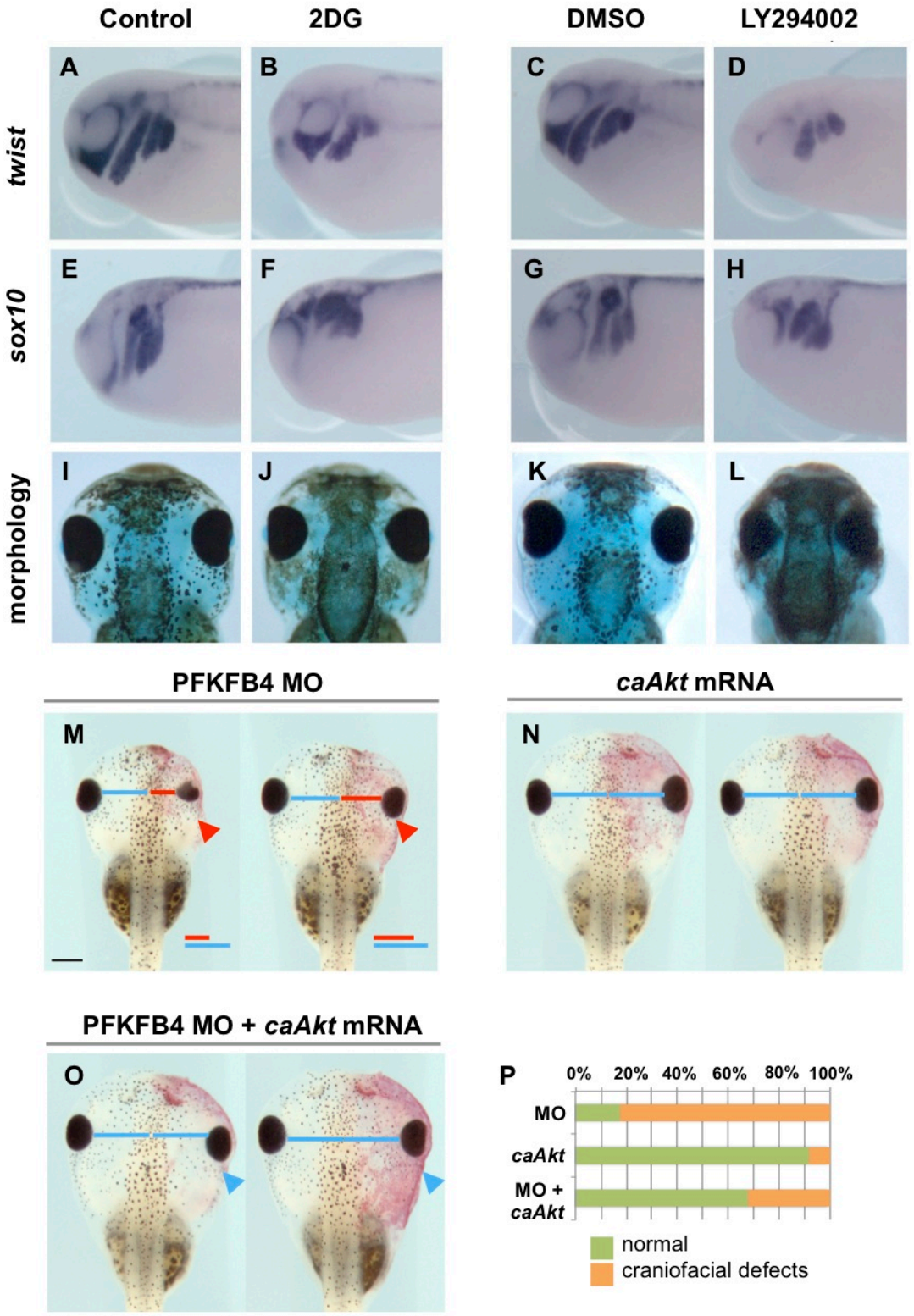

bioRxiv preprint doi: https://doi.org/10.1101/168807; this version posted July 26, 2017. The copyright holder for this preprint (which was not certified by peer review) is the author/funder. All rights reserved. No reuse allowed without permission.

Fig 8

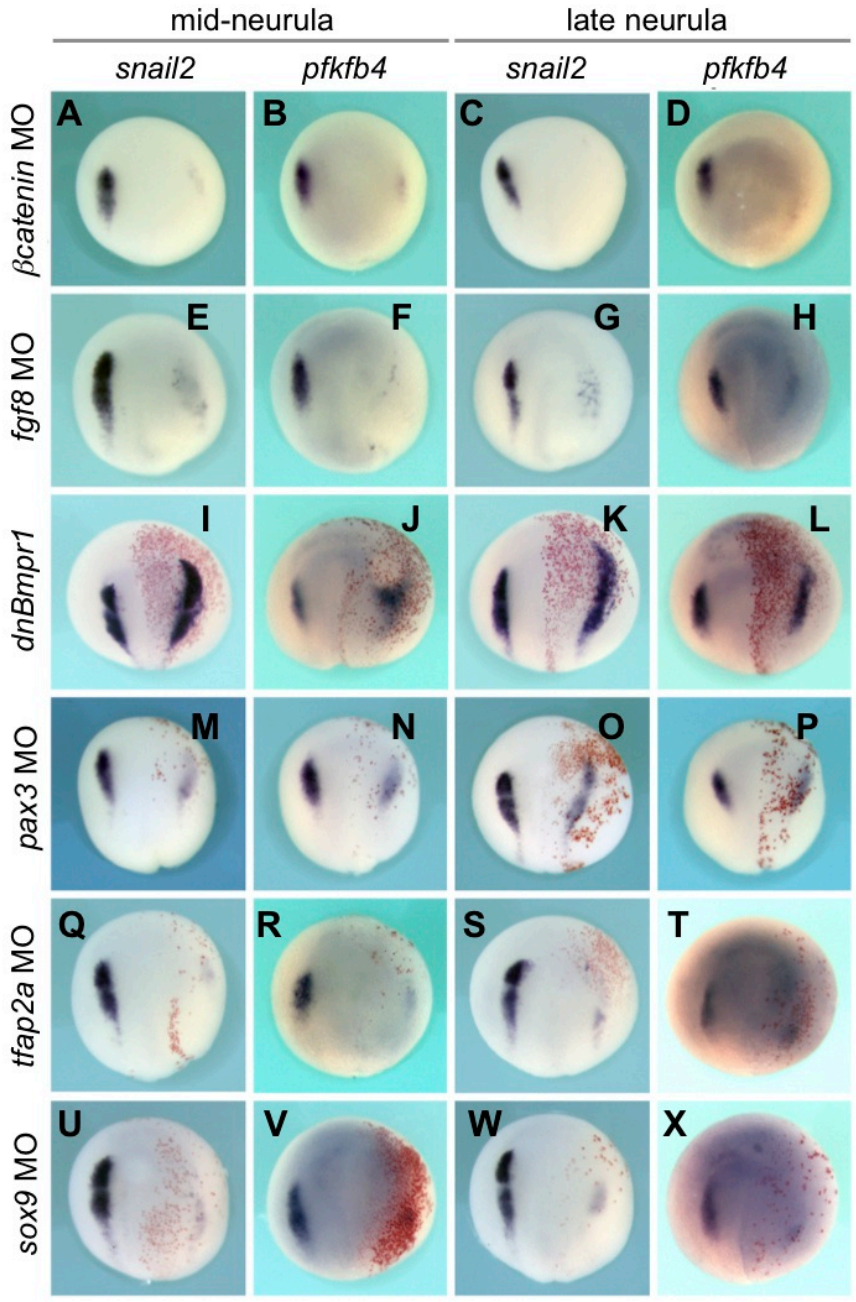

bioRxiv preprint doi: https://doi.org/10.1101/168807; this version posted July 26, 2017. The copyright holder for this preprint (which was not certified by peer review) is the author/funder. All rights reserved. No reuse allowed without permission.

Fig. 9

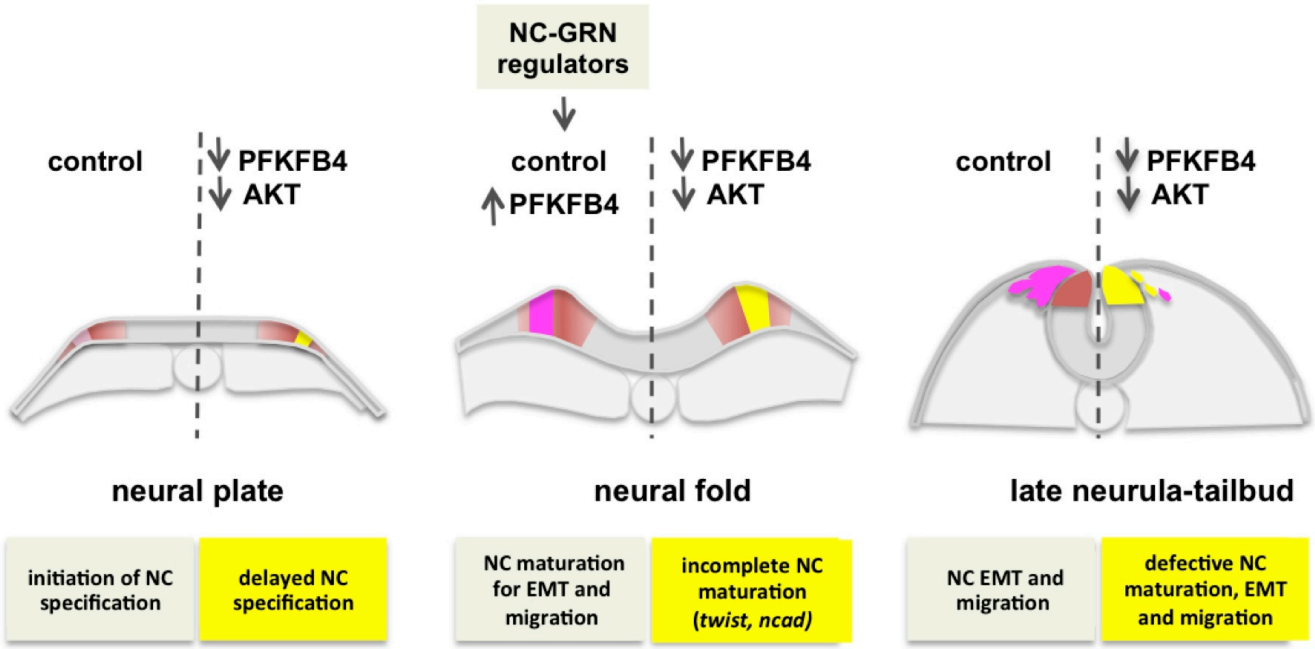

bioRxiv preprint doi: https://doi.org/10.1101/168807; this version posted July 26, 2017. The copyright holder for this preprint (which was not certified by peer review) is the author/funder. All rights reserved. No reuse allowed without permission.

Table S1

Reagents used in this study

Plasmids

Plasmid	Reference	usage
caBmpr1	Gift from R. Harland	mRNA
dnBmpr1	(Graff et al. 1994)	mRNA
caAkt	(Peyssonnaux et al. 2000)	mRNA
cmyc	(Bellmeyer et al, 2003)	WISH probes
Epidermal Keratin K81	(Bradley et al. 1998)	WISH probes
Fgf8	(Monsoro-Burq et al. 2003)	mRNA
Hes4	(Nichane et al, 2008)	WISH probes
Histone2B-GFP	(Tsien 1998)	mRNA
Hoxb9	(Sharpe et al. 1988)	WISH probes
Myod	(Hopwood et al. 1989b)	WISH probes
Msx1	(Suzuki et al, 1997)	WISH probes
nLacZ	(Gammill & Sive 2000)	mRNA
Otx2	(Lamb et al. 1993)	WISH probes
Pax3	(Monsoro-Burq et al. 2005)	WISH probes
Pfkfb1	(Pegoraro et al. 2013)	WISH probes
Pfkfb3	(Pegoraro et al. 2013)	WISH probes
Pfkfb4	(Pegoraro et al. 2013; Pegoraro et al. 2015)	mRNA; WISH probes
Snai2	(Grammer et al. 2000)	WISH probes
Sox2	(Mizuseki et al. 1998)	WISH probes
Sox9	(Spokony et al. 2002)	WISH probes
Sox10	(Aoki et al. 2003)	WISH probes
Tfap2a	(de Crozé et al. 2011)	mRNA
Twist	(Hopwood et al. 1989a)	WISH probes
Wnt7b	(Grammer et al. 2000)	mRNA
Zic1	(Mizuseki et al. 1998)	WISH probes

Morpholinos

Morpholino	Sequence
βcatenin MO	(Heasman et al. 2000)
Fgf8 MO	(Monsoro-Burq et al. 2003)
Pax3 MO	(Monsoro-Burq et al. 2005)
Pfkfb4 MO	(Pegoraro et al. 2015)
SensePhoto-xlPfkfb4_MO	AAAGGTAATGGPTTGTGGGATGG
Tfap2a MO	(Luo et al. 2003)
Sox9 MO	(Spokony et al. 2002)

bioRxiv preprint doi: https://doi.org/10.1101/168807; this version posted July 26, 2017. The copyright holder for this preprint (which was not certified by peer review) is the author/funder. All rights reserved. No reuse allowed without permission.

Primers for quantitative real-time PCR

qRT-PCR Primer pair	Fwd/ rev	Sequence	Reference
EF1alpha	Fwd Rev	ACACTGCTCACATTGCTTGC AGAAGCTCTCCACGCACATT	(Pegoraro et al. 2015)
Epidermal Keratin K81	Fwd Rev	GGAGGGAGGACTGGGACAGGTGAC GAAACAACCTTCCCATCAACCACCT	(Pegoraro et al. 2015)
FoxD3	Fwd Rev	GTGCGTCCCCTTGTCAAGAA TGCGAGTGCCTTCAAATCCT	This study
MyoD	Fwd Rev	TACACTGACAGCCCCAATGA TGCAGAGGAGAACAGGGACT	(Krieg et al. 1989)
N-cadherin	Fwd Rev	CTGGCAGCAGGACTAGACAG GGGTTTCCTTCCATGTCCGT	This study
ODC	Fwd Rev	CATGGCATTCTCCCTGAAGT TGGTCCCAAGGCTAAAGTTG	(Milet et al. 2013)
Pax3	Fwd Rev	CAAGCTCACAGAGGCGCGAGT AGCTGGCATAGCTGCAGGAGG	(Pegoraro et al. 2015)
Pfkfb1	Fwd Rev	AGTGCTGAAACTGACCCCTG TCATCTGGCTCACGGGAAAC	(Pegoraro et al. 2013)
Pfkfb2	Fwd Rev	TGTCGGGAGGATTGGAGGAGATTCA GACACACCAAGGGCTTCTGCCGT	(Pegoraro et al. 2013)
Pfkfb3	Fwd Rev	GCTGAGAGTGGCTGCGGCTT TGGAATCTGAGTGTGTGGACCCT	(Pegoraro et al. 2013)
Pfkfb4-3	Fwd Rev	TGGAATCTGAGTGTGTGGACCCT CGGTTGCCTCCTCGCTGCTAC	(Pegoraro et al. 2013)
Snai2	Fwd Rev	CACACGTTACCCTGCGTATG TCTGTCTGCGAATGCTCTGT	(Nichane et al. 2008)
Twist	Fwd Rev	AATGCCACTACAGCTCAGGC GCCCTTTCTCCCTTTAACGC	(Plouhinec et al. 2014)

Antibodies

Antibody	Reference	Host	Dilution	Usage
Anti-actin	Sigma # A2066	Rabbit	1/2000	WB
Anti-Akt	Cell signaling #9272	Rabbit	1/1000	WB
Anti-cleaved Caspase-3 (D175)	Cell signaling #9661L	Rabbit	1/500	IHC
Anti-digoxigenin-AP	Roche #11 093 274 910	sheep	1/4000	WISH
Anti-GFP Living Colors A.v. Peptide Antibody	Clontech #632377	Rabbit	1/500	IF
Anti-phospho-Akt(Ser472)(D9E)XP	Cell signaling #4060S	Rabbit	1/2000	WB
Alkaline Phosphatase AffiniPure Goat Anti-Rabbit IgG (H+L)	Jackson ImmunoResearch #111-035-003	Rabbit	1/500	IHC
Peroxidase conjugated affiniPure Goat anti-Rabbit-IgG (H+L)	Jackson ImmunoResearch #111-055-003	Rabbit	1/200000	WB

Pharmacological treatments and lactate dosage

Pharmacological reagents /kits	Reference	Concentration	usage
LY294002	Sigma #L9908	40μM-80μM	PI3K/Akt blockade assay
2-Deoxyglucose	Sigma #D8375	100-200mM	Glycolysis blockade assay

bioRxiv preprint doi: https://doi.org/10.1101/168807; this version posted July 26, 2017. The copyright holder for this preprint (which was not certified by peer review) is the author/funder. All rights reserved. No reuse allowed without permission.

UO126	Sigma #19147	40-80μM	MAPK/Erk inhibition
L-Lactate Assay Kit	Abcam #AB65330		Lactate dosage
Click-iT EdU Alexa Fluor 555 Imaging kit	Invitrogen #C10338		Proliferation assay

bioRxiv preprint doi: https://doi.org/10.1101/168807; this version posted July 26, 2017. The copyright holder for this preprint (which was not certified by peer review) is the author/funder. All rights reserved. No reuse allowed without permission.

873 **SUPPLEMENTARY FIGURES LEGENDS.**

874

875 **Fig. S1. Schematics of glycolysis.** Glucose phosphorylation by hexokinase is the first irreversible
876 step of glycolysis. The second and rate-limiting step of glycolysis is catalyzed by PFK1. This step is
877 tightly controlled in cells, by the levels of Fructose-2.6-bisphosphate, potent allosteric regulator of
878 PFK1. Fructose-2.6-bisphosphate is synthesized by PFKFB1-4 enzymes, which thus control the rate
879 of glycolysis in the cells. PFKFB3 and PFKFB4, with a strong kinase activity over their phosphatase
880 activity, promote Fructose-2.6-bisphosphate synthesis and stimulate glycolysis. In addition to their
881 classic role in glycolysis regulation, recent unconventional roles of the PFKFB enzymes have been
882 described in cancer or development (see text).

883

884 **Fig. S2. *Pfkfb4* is specifically upregulated in the neural border and neural crest during**
885 **neurulation.** (A-J). Transverse sections through the anterior neural plate at mid and late neurula
886 stages (stage 14 and 18, respectively) allow comparing *Snail2* and *Pfkfb4* expression in the neural
887 crest (*Snail2* and *Pfkfb4*), neural plate (*Pfkfb3*) and somites (*Pfkfb1*). (A,F): The notochord, neural
888 plate and paraxial mesoderm are outlined on hematoxylin-eosin stained paraffin sections. (B-E,G-J)
889 Vibratome sections of WISH-stained embryos. The arrow indicates the midline and the notochord.
890 The blue arrowheads indicate in situ hybridization staining position. Red bar positions the neural
891 border at stage 14. Scale bar = 200μm. (K) A quantitative analysis of *Xenopus laevis Pfkfb1-4*
892 expression levels shows that *Pfkfb4* is specifically enriched at the neural border of frog neurulas (red),
893 compared to the anterior neural fold (yellow). All values are normalized to *Odc* expression and to the
894 average expression in a sibling whole embryo lysed at late neurula stage 18 (blue, value = 1). *Snail2*
895 expression is used to monitor the quality of dissected tissues and shows high and specific expression
896 at the neural border.

897 **Fig. S3. Patterning defects in NC are not due to increased cell death, after low-level PFKFB4**
898 **depletion in vivo.** In this study, we use a low-level depletion of PFKFB4, with reduced MO
899 concentrations, in order to bypass the earlier developmental arrest observed in previous study, when
900 PFKFB4 severely depleted (above 60% mRNA depletion) and prevents gastrulating ectoderm
901 specification (Pegoraro et al., 2015). Importantly, this severe depletion was rescued by adding back a
902 MO-resistant *pfkfb4* mRNA, assessing both MO specificity and lack of non-specific toxicity (Pegoraro
903 et al., 2015). (A) Here, we check that the morphant cells do not undergo elevated cell death at later
904 stages of development by analyzing mid-neurulas at stage 14 and the end of neurulation stage 18. (B-
905 C) We find less than 30% of embryos with caspase-positive cells in the lacZ-injected area (B), in

bioRxiv preprint doi: https://doi.org/10.1101/168807; this version posted July 26, 2017. The copyright holder for this preprint (which was not certified by peer review) is the author/funder. All rights reserved. No reuse allowed without permission.

conditions when over 70% of sibling embryos show deficient *twist* expression (C, either "strong", "moderate" or "mild" decrease). The number of caspase-positive cells is slightly more elevated than in uninjected or lacZ-only-injected embryos, or in ventrally-injected morphants, but it remains limited to few cells and cannot account for the incidence of the patterning defects. Representative exemples of the majoritary phenotypes are shown for each condition, i.e. "rare" or "+/-" phenotypes. Embryos analyzed in this experiments: uninjected, n=49; lacZ-injected, n=46; PFFB4misMO-injected, n=16; PFKFB4MO-injected, n=43.

Fig. S4. PFKFB4 is required for neural crest migration. (A,D) WISH analysis of neural crest migration at tadpole stages. When *Pfkfb4* MO is injected, embryos display decreased *Twist* expression and neural crest migration defects (B), when compared to control embryos (A). (C) In contrast, the co-injection of *Pfkfb4* mRNA with *Pfkfb4* MO restores *Twist* expression and NC migration, showing that the neural crest migration defects are due to PFKFB4 knowckdown. A-C are side views, anterior is to the right.

Fig. S5.PFKFB4 depletion and 2DG treatment block glycolysis, LY294002 blocks AKT phosphorylation. (A) PFKFB4 low-level depletion affects lactate levels in embryos, indicating efficient glycolysis blockade. (B, C) Lactate concentration and Akt phosphorylation were decreased following 2-DG or LY294002 treatment (LY, two doses 60-80 μM), respectively. Error bars represent s.e.m (t-test $p<0.05$). (C,D) Blocking glycolysis during neurulation, between st. 14 and st. 18 does not affect *twist* expression *in vivo*. (D) control and (E) 2DG-treated embryos displayed normal *twist* expression (n=15 each).

Fig. S6. Glycolysis and PI3K-Akt signaling control neural crest migration. Glycolysis blockade (A-J) and PI3K-Akt blockade (K-T) during EMT and neural crest migration (stage 18 to stage 24) affects neural crest migration as shown by the expression of *Sox9*, *Sox10* and *Twist*. Embryos rinsed at stage 24 and grown until stage 45 display craniofacial and eye development defects, albeit the presence of all individual cartilage elements. (A-C,F-H,K-M,P-R, U-W) Side views, anterior is to the left. (D,I,N,S,X) dorsal views st 45. (E,J,O,T,Y) Ventral views of alcian blue stained visceral cartilages, st 45. Scale bar= 500μm.

Fig. S7. *Pfkfb4* is regulated by the neural crest gene regulatory network. Unilateral overexpression of members of the neural crest gene regulatory network modulates *Pfkfb4* expression at mid and late neurula stages (stage 14 and 18, respectively). (A-D) Overexpression of WNT signals

bioRxiv preprint doi: https://doi.org/10.1101/168807; this version posted July 26, 2017. The copyright holder for this preprint (which was not certified by peer review) is the author/funder. All rights reserved. No reuse allowed without permission.

940 increases both Snail2 and Pfkfb4 expression. (E-H) FGF8 overexpression results in complete loss of
941 *pfkfb4*, while *snai2* is expanded. (I-L) BMP overexpression with a constitutively active form of BMPR1
942 results in loss of *Snail2* and *Pfkfb4* expression in the NC and ectopic expression in the neural plate.
943 (M-T) PAX3 and TFAP2a positively regulate *Pfkfb4* expression, similarly to *Snail2*. Dorsal views,
944 anterior is to the top. Scale bar = 500μm.

bioRxiv preprint doi: https://doi.org/10.1101/168807; this version posted July 26, 2017. The copyright holder for this preprint (which was not certified by peer review) is the author/funder. All rights reserved. No reuse allowed without permission.

Fig. S1

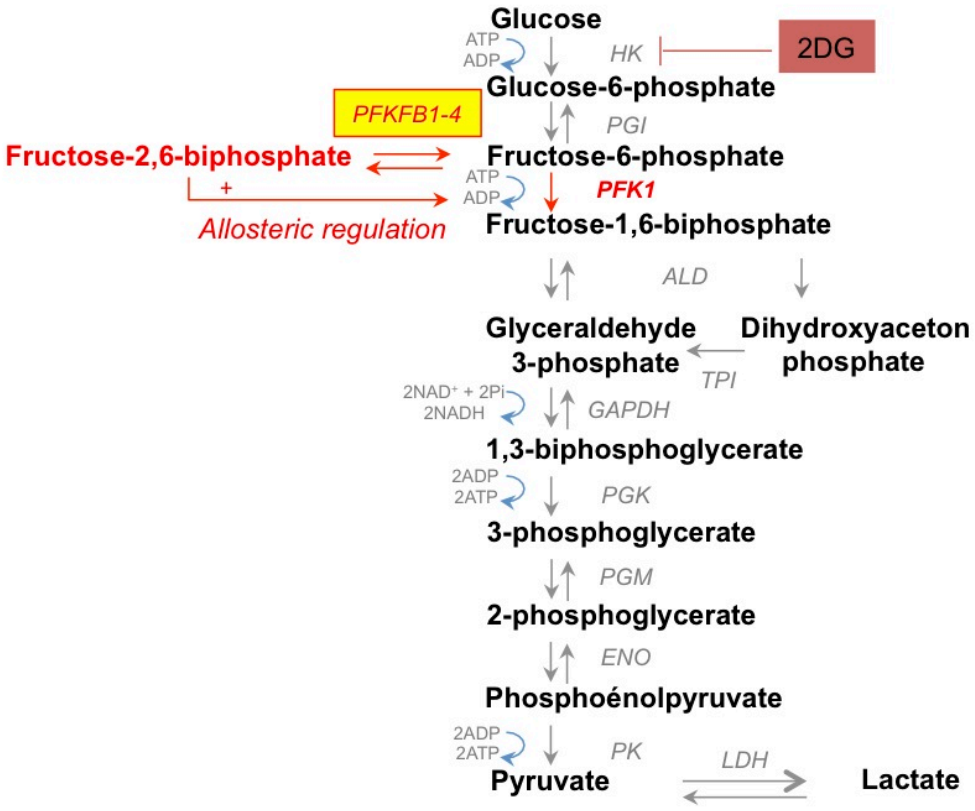

bioRxiv preprint doi: https://doi.org/10.1101/168807; this version posted July 26, 2017. The copyright holder for this preprint (which was not certified by peer review) is the author/funder. All rights reserved. No reuse allowed without permission.

Fig. S2

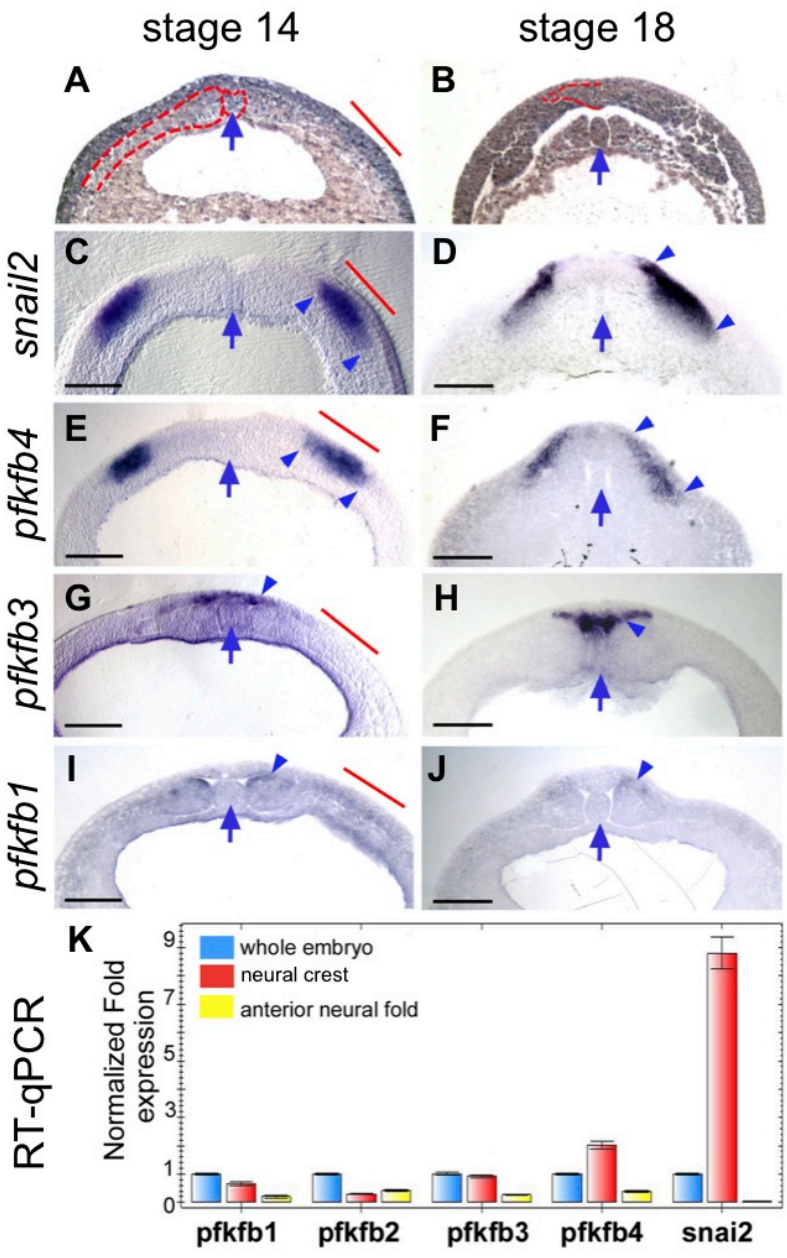

bioRxiv preprint doi: https://doi.org/10.1101/168807; this version posted July 26, 2017. The copyright holder for this preprint (which was not certified by peer review) is the author/funder. All rights reserved. No reuse allowed without permission.

Fig. S3

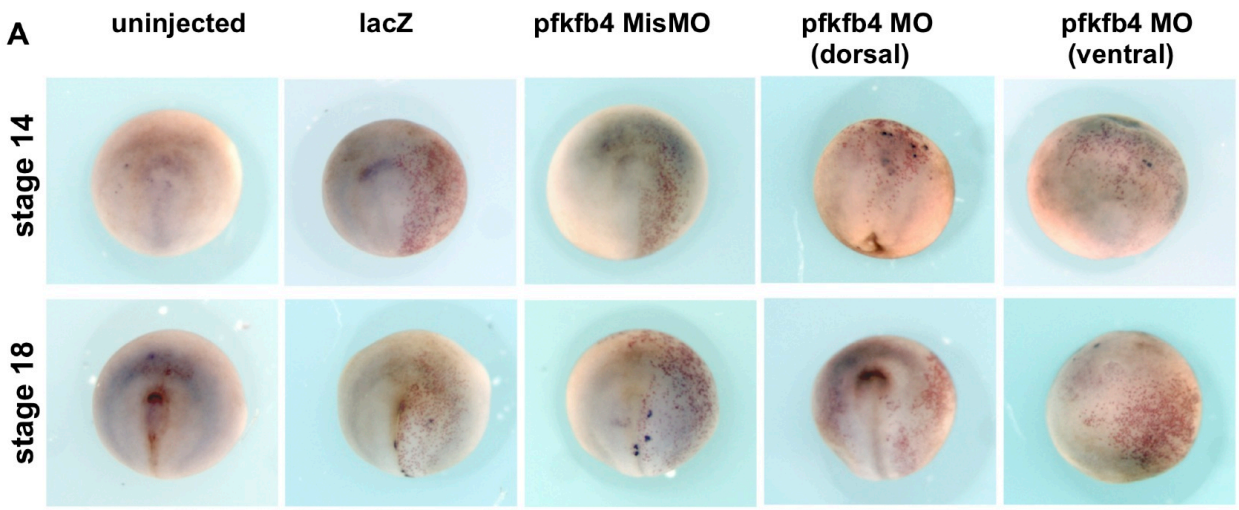

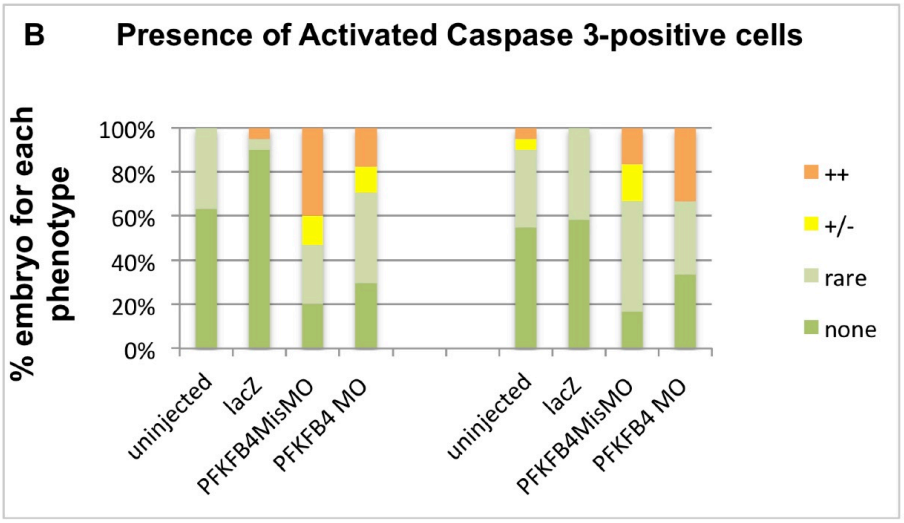

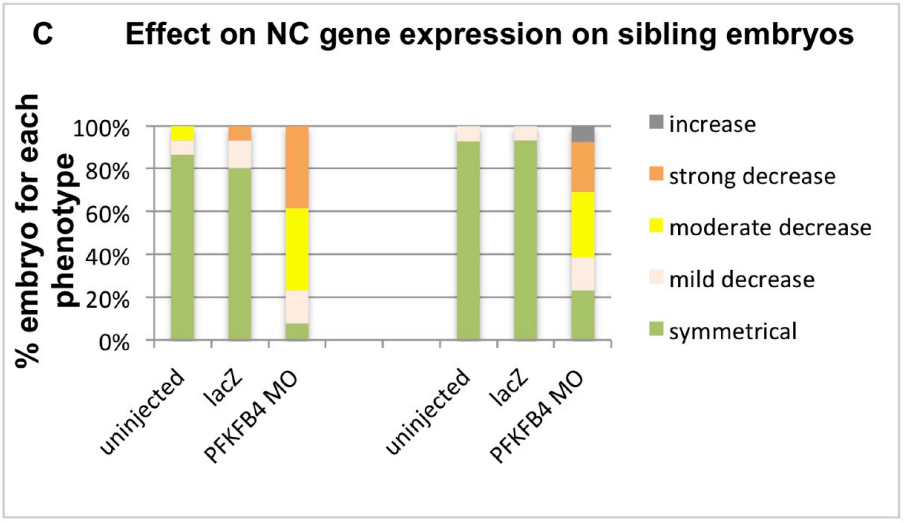

bioRxiv preprint doi: https://doi.org/10.1101/168807; this version posted July 26, 2017. The copyright holder for this preprint (which was not certified by peer review) is the author/funder. All rights reserved. No reuse allowed without permission.

Fig S4

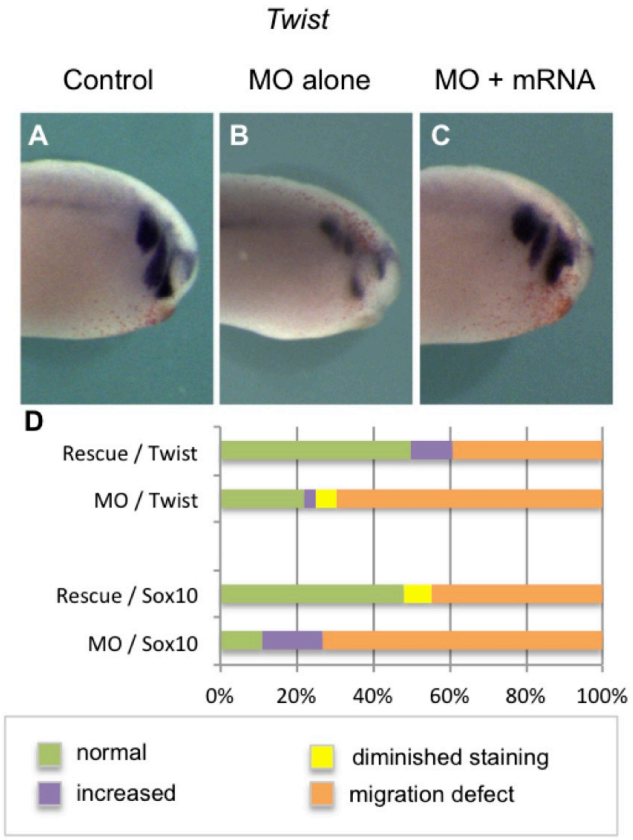

bioRxiv preprint doi: https://doi.org/10.1101/168807; this version posted July 26, 2017. The copyright holder for this preprint (which was not certified by peer review) is the author/funder. All rights reserved. No reuse allowed without permission.

Fig. S5

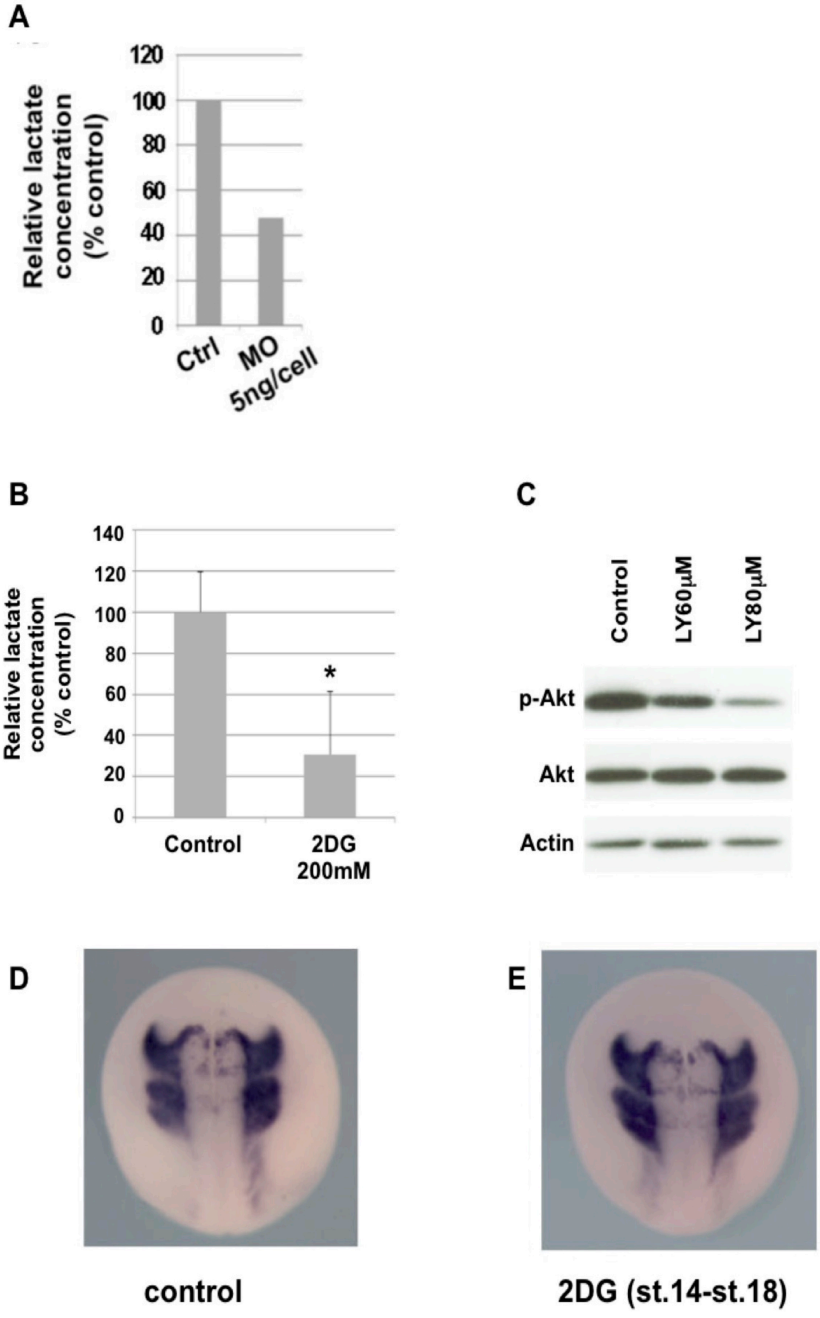

bioRxiv preprint doi: https://doi.org/10.1101/168807; this version posted July 26, 2017. The copyright holder for this preprint (which was not certified by peer review) is the author/funder. All rights reserved. No reuse allowed without permission.

Fig S6

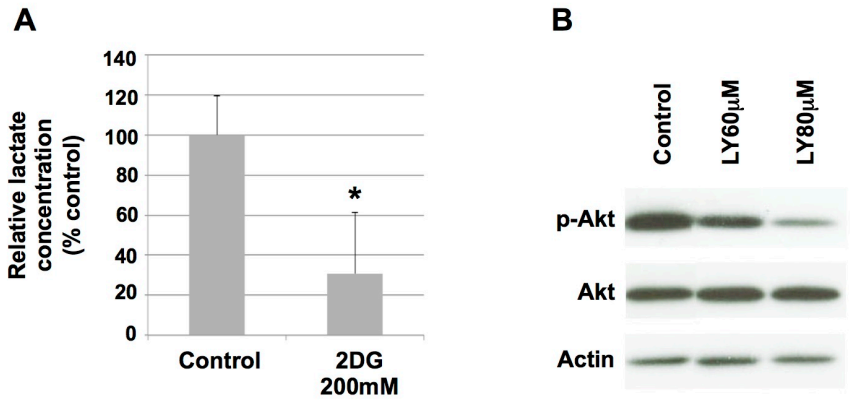

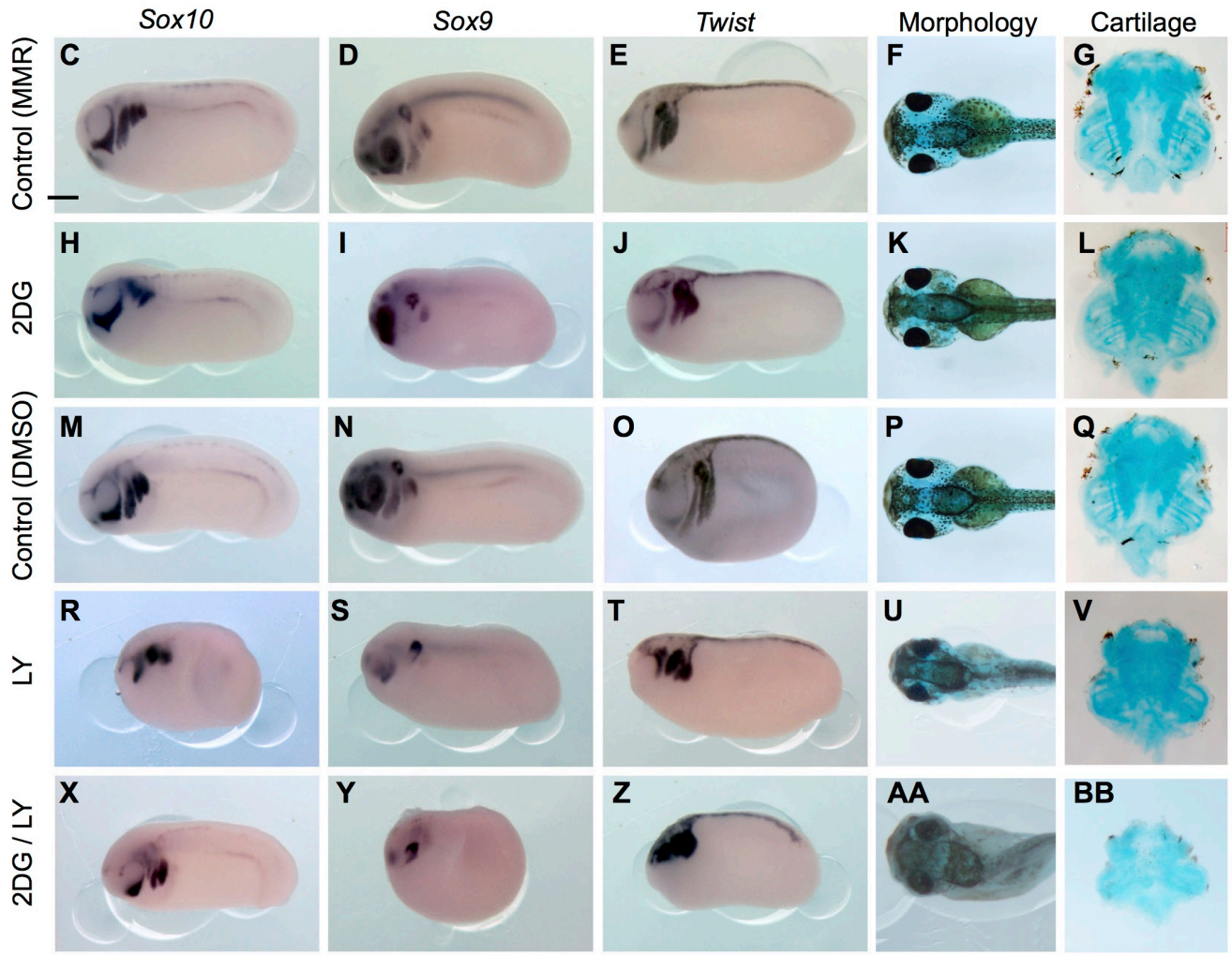

bioRxiv preprint doi: https://doi.org/10.1101/168807; this version posted July 26, 2017. The copyright holder for this preprint (which was not certified by peer review) is the author/funder. All rights reserved. No reuse allowed without permission.
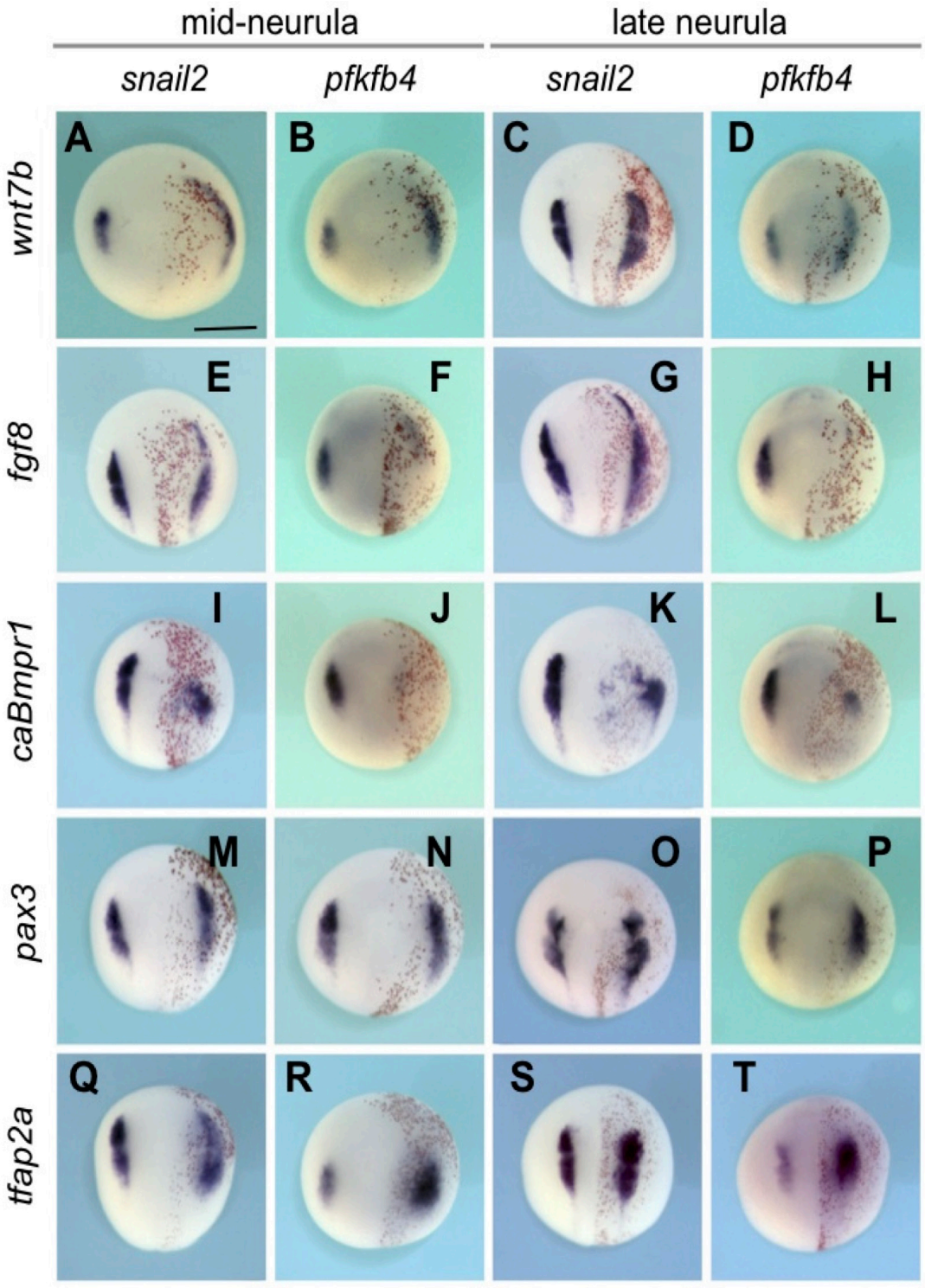
Fig. S7